Urban Canopy Modeling of the New York City Metropolitan Area: A Comparison and Validation of Single- and Multilayer Parameterizations

TEDDY HOLT AND JULIE PULLEN

Marine Meteorology Division, Naval Research Laboratory, Monterey, California

(Manuscript received 9 May 2006, in final form 28 July 2006)

ABSTRACT

High-resolution numerical simulations are conducted using the Coupled Ocean–Atmosphere Mesoscale Prediction System (COAMPS)[1] with two different urban canopy parameterizations for a 23-day period in August 2005 for the New York City (NYC) metropolitan area. The control COAMPS simulations use the single-layer Weather Research and Forecasting (WRF) Urban Canopy Model (W-UCM) and sensitivity simulations use a multilayer urban parameterization based on Brown and Williams (BW-UCM). Both simulations use surface forcing from the WRF land surface model, Noah, and hourly sea surface temperature fields from the New York Harbor and Ocean Prediction System model hindcast. Mean statistics are computed for the 23-day period from 5 to 27 August (540-hourly observations) at five Meteorological Aviation Report stations for a nested 0.444-km horizontal resolution grid centered over the NYC metropolitan area. Both simulations show a cold mean urban canopy air temperature bias primarily due to an underestimation of nighttime temperatures. The mean bias is significantly reduced using the W-UCM (-0.10°C for W-UCM versus -0.82°C for BW-UCM) due to the development of a stronger nocturnal urban heat island (UHI; mean value of 2.2°C for the W-UCM versus 1.9°C for the BW-UCM). Results from a 24-h case study (12 August 2005) indicate that the W-UCM parameterization better maintains the UHI through increased nocturnal warming due to wall and road effects. The ground heat flux for the W-UCM is much larger during the daytime than for the BW-UCM (peak ~300 versus 100 W m^{-2}), effectively shifting the period of positive sensible flux later into the early evening. This helps to maintain the near-surface mixed layer at night in the W-UCM simulation and sustains the nocturnal UHI. In contrast, the BW-UCM simulation develops a strong nocturnal stable surface layer extending to approximately 50–75-m depth. Subsequently, the nocturnal BW-UCM wind speeds are a factor of 3–4 less than W-UCM with reduced nighttime turbulent kinetic energy (average < 0.1 m^2 s^{-2}). For the densely urbanized area of Manhattan, BW-UCM winds show more dependence on urbanization than W-UCM. The decrease in urban wind speed is most prominent for BW-UCM both in the day- and nighttime over lower Manhattan, with the daytime decrease generally over the region of tallest building heights while the nighttime decrease is influenced by both building height as well as urban fraction. In contrast, the W-UCM winds show less horizontal variation over Manhattan, particularly during the daytime. These results stress the importance of properly characterizing the urban morphology in urban parameterizations at high resolutions to improve the model's predictive capability.

1. Introduction

The New York City (NYC) metropolitan area has a highly developed urban landscape that is known to generate a pronounced urban heat island (UHI) whereby at night the city acts as a heat reservoir relative to the surrounding rural environment. In the NYC metropolitan area the UHI effect is strongest near the surface and estimated to be 2°–5°C (Bornstein 1968; Gedzelman et al. 2003). Urban-induced atmospheric circulations, though typically small scale, can have a significant impact on mesoscale dynamics. For example, synoptic and sea-breeze frontal passages can be retarded due to frictional effects by 50% as they approach NYC (Loose and Bornstein 1977; Bornstein and Thompson 1981). Urban heating also appears to play a role in distorting near-surface temperatures as sea-breeze fronts pass (Novak and Colle 2006). Also, summer thunderstorm

[1] COAMPS is a registered trademark of the Naval Research Laboratory.

Corresponding author address: Dr. Teddy R. Holt, Marine Meteorology Division, Naval Research Laboratory, 7 Grace Hopper Ave., Monterey, CA 93943.
E-mail: holt@nrlmry.navy.mil

DOI: 10.1175/MWR3372.1

lines have been observed to bifurcate and go around the metropolitan region in response to localized urban-induced convection (Bornstein and LeRoy 1990).

The NYC urban environment presents a notable forecasting challenge for mesoscale models because of (i) the tremendous horizontal and vertical variability of the urban landscape and (ii) the variety of surface forcing. For example, the buildings for a 4-km^2 area centered near Rockefeller Center in midtown Manhattan have an average height of 53 m, but a standard deviation of 47 m, illustrating the highly corrugated skyline. In contrast, the more residential areas of Chelsea and Greenwich Village less than 5 km to the south of midtown have an average building height of less than 20 m. Less than 5 km to the north of the highly urbanized midtown is the huge vegetative and forested area of Central Park (CPK). The surface forcing varies across the metropolitan area from shallow rivers (East and Hudson Rivers) flanking Manhattan that typically heat and cool rather quickly, to the deeper coastal bays and sounds that typically retain heat longer. Also, the coastline is highly irregular with strong ocean bathymetric variations over tens of kilometers. While there are few trees and vegetative surfaces in Manhattan other than CPK, the suburban boroughs have large variability in trees and vegetation cover that modify surface heat fluxes.

The heterogeneous surface properties create localized areas of heating and cooling, wind circulations, and moisture deficits and surpluses that are typically subgrid scale for operational mesoscale models. As such, these urban and land surface effects must be parameterized. Parameterizations in state-of-the-art mesoscale models are either single- or multilayer. Single-layer schemes can be as simple as modifications to the surface characteristics of the urban landscape (Liu et al. 2006; Grossman-Clarke et al. 2005; Childs and Raman 2005; Uno et al. 1995; Avissar and Pielke 1989) or more sophisticated urban models such as Kusaka et al. (2001), Masson (2000), and Mills (1997). These models have been shown to accurately predict surface fluxes, temperatures, and net radiation for case studies of UHIs (Kusaka et al. 2001). Multilayer schemes include Brown and Williams (1998), Vu et al. (1999), Ca et al. (2002), Martilli et al. (2002), and Chin et al. (2005). These schemes can be as simple as modifications to predictive equations to include urban effects (i.e., Brown and Williams 1998; Chin et al. 2005) or more detailed to include predictive equations for roof and wall values, incorporating complex radiative effects such as shadowing and reflection at multiple levels within the urban canopy (i.e., Kusaka et al. 2001; Martilli et al. 2002).

The context of the current model parameterization study is the August 2005 field program of the NYC Urban Dispersion Program (UDP) sponsored by the Department of Homeland Security (DHS). The field program was conducted from 5 to 27 August in midtown Manhattan. The program's primary objective is to study how air flows in a city environment. Field program data will be used in the future to improve and validate numerical models that simulate the atmospheric movement of tracers within cities, and around, into, and within building interiors. In support of the field program, several numerical weather prediction models were run at Stony Brook University and the Naval Research Laboratory (NRL), both in ensemble and deterministic mode, to provide guidance for positioning of passive tracer releases at street level. These models contain a variety of surface parameterizations, ranging from bare soil surface hydrology with no urban parameterization to coupled vegetative and single- or multilayer urban parameterizations. Ongoing work is focused on comparing and validating these model results and their parameterizations.

The aim of this study is to assess the impact of two fundamentally different urban parameterizations in a mesoscale model for long-term (23 day) hindcast simulations. Single- and multilayer urban parameterizations have been used in episodic case studies (e.g., Kusaka and Kimura 2004a; Chin et al. 2005), but not for longer-term simulations under varying synoptic and mesoscale forcing. By accurately representing the time-varying, high-resolution land and ocean features that influence the NYC metropolitan area atmospheric circulation, we seek to illuminate aspects of the near-surface and boundary layer response to different representations of urban forcing. In section 2 the modeling system is described, including pertinent urban modeling aspects. In section 3 we discuss the validation of simulations with observations from the 23-day time period along with mean statistics. In section 4, we describe the spatially heterogeneous aspects of the atmospheric response for an urban versus a vegetated site for a high heat day with afternoon sea-breeze penetration into Manhattan. Included is an investigation of the differences in near-surface urban energy budgets and dynamical forcing for the two urban parameterizations.

2. Modeling system

a. Coupled Ocean–Atmosphere Mesoscale Prediction System (COAMPS) configuration

The atmospheric component of NRL's COAMPS (Hodur 1997; more information is available online at http://www.nrlmry.navy.mil/coamps-web/web/home/)

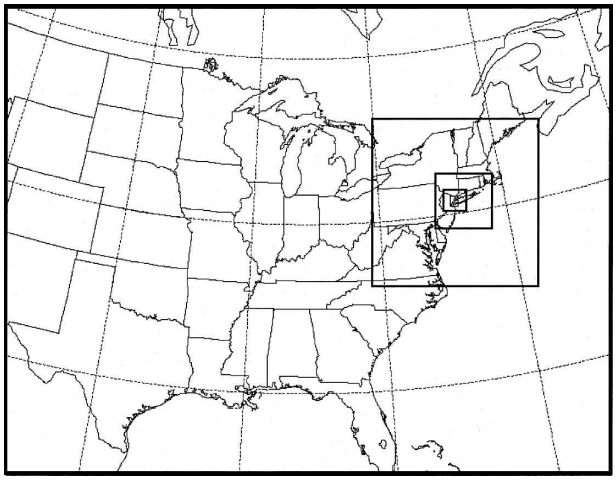

FIG. 1. COAMPS nests 1 (36 km), 2 (12 km), 3 (4 km), 4 (1.33 km), and 5 (0.444 km) domains.

with nonhydrostatic dynamics is used for the numerical model simulations. For this study COAMPS is configured for a U.S. east coast five-nest, one-way-interactive domain of 36-, 12-, 4-, 1.33-, and 0.444-km resolutions focused on the island of Manhattan with 110×85, 91×91, 91×91, 106×106, and 106×166 grid points for the five nests, respectively (Fig. 1). The emphasis is on the highest-resolution 0.444-km nest, so subsequent figures and discussion, with the exception of the synoptic discussion, will pertain to nest 5. The model has 45 vertical sigma-z levels from 10 to 26 015 m with increased vertical resolution in the lower levels. There are 14 levels below 900 m, with the lowest four levels at 10, 30, 52.5, and, 80 m above ground level (AGL).

A series of 12-h simulations are conducted for 23 days (5–27 August 2005). The first simulation starting at 0000 UTC 5 August 2005 uses initial fields interpolated from the 1° Navy Operational Global Atmospheric Prediction System (NOGAPS) to the COAMPS domain. All subsequent forecasts use the previous COAMPS 12-h forecast as initial conditions. At the beginning of each assimilation cycle (every 12 h), a three-dimensional multivariate optimum interpolation using quality-controlled data from radiosondes, surface stations, aircraft, and satellites is conducted to obtain an analysis blended from the observations and model first guess (Hodur 1997). The outermost 36-km nest receives boundary conditions from NOGAPS at a 6-h interval.

Planetary boundary layer and subgrid-scale turbulence processes in COAMPS are represented by a turbulent kinetic energy (TKE) scheme following Mellor and Yamada (1982), with the surface layer parameterized after Louis et al. (1982). The Weather Research and Forecasting (WRF) land surface–hydrology model, Noah (Pan and Mahrt 1987; Chen et al. 1996; Chen and Dudhia 2001; Ek et al. 2003; Holt et al. 2006), is based on the coupling of the diurnally dependent Penman potential evaporation approach of Mahrt and Ek (1984), the multilayer soil model of Mahrt and Pan (1984), and the one-layer canopy model of Pan and Mahrt (1987), and is initialized from August 2005 climatological ground surface wetness, assuming a constant vertical profile, and from climatological surface and deep soil temperatures. An alternative method of soil initialization would be to use observation-based analyses to drive the land surface model (LSM) in a decoupled mode on the same grids as used in the coupled simulations (Holt et al. 2006; Chen et al. 2004a). Unfortunately, long-term (~12–18 month) observation-based analyses were not available. A less desirable method is to interpolate from coarser-resolution operational analyses such as the National Centers for Environmental Prediction (NCEP) 40-km Eta Data Assimilation System. However, mismatches in terrain height, land use, and soil texture can often result in the degradation of model forecast skill (Chen et al. 2004a). Thus, because the focus is on areas where the land use is urban and the surface typically impervious, the use of climatological soil conditions that have consistent soil profiles can be justified.

The radiation scheme is that of Harshvardhan et al. (1987). Moist processes on the 36- and 12-km nests are simulated using a modified Kain and Fritsch (1993) cumulus parameterization, but are treated explicitly on nests 3, 4, and 5 with a modified Rutledge and Hobbs (1983) and Khairoutdinov and Kogan (2000) moist physics parameterization, which includes graupel.

Analyzed SSTs on the outer three nests are derived from an optimum interpolation of available satellite and in situ data as in operational COAMPS applications (Chen et al. 2003). When data are scarce these analyzed SSTs tend to be smooth, and this is particularly true when the domain is very small. Thus, for nests 4 and 5, SSTs are interpolated to the COAMPS grid from hourly New York Harbor Ocean Prediction System (NYHOPS) ocean model hindcast fields. NYHOPS is a version of the Princeton Ocean Model (Blumberg and Mellor 1987; Bruno and Blumberg 2004) with 11 vertical sigma levels and atmospheric forcing from the NCEP Eta 12-km atmospheric fields. The domain extends out to the continental shelf break where the resolution is ~25 km, and inshore to the New York–New Jersey estuary region where the resolution reaches ~500 m. Operationally the system is run in real time to provide water levels, ocean temperatures, and currents for shipping and search-and-rescue applica-

tions. NYHOPS includes tides and hourly discharge measured at the U.S. Geological Survey (USGS) river gauges. In addition, effluents from 110 waste water treatment plants obtained from the Interstate Sanitation Commission, and approximate urban drainage discharges are introduced at point sources in the domain. These discharges specified within NYHOPS render the modeled coastal and estuarine water temperatures more heterogeneous, in accordance with observations. An extensive comparison with in situ measurements of temperature, salinity, and water level showed high skill levels for NYHOPS (Fan et al. 2006).

Pullen et al. (2007) show that these time-varying SSTs, relative to the operationally specified (control) SSTs, have a positive impact on forecast skill in the COAMPS modeling system described here. In particular, utilizing high-resolution NYHOPS SSTs reduced the wind speed mean bias at three coastal stations. Dynamically, areas of cold upwelled water occurring in the NYHOPS SSTs but not in the control SSTs influenced the atmosphere through internal boundary layer formation whose temporal evolution matched the observations.

b. Urban canopy modeling

To represent the effects of the city on the mesoscale, an urban canopy parameterization is used on nests 4 and 5. Two different parameterizations are used for the 23-day simulations: the single-layer WRF Urban Canopy Model (W-UCM) based on Kusaka et al. (2001) and the multilayer parameterization based on Brown and Williams (1998; BW-UCM). The original implementation of BW-UCM has been modified in COAMPS by Chin et al. (2005) to include a rooftop surface energy equation, and that is the implementation used here. These two parameterizations have been described extensively in the literature so appendixes A and B provide only basic details on the model equations and parameters used in the parameterizations. The default values for both parameterizations as described in the literature are used and no attempt has been made to optimize or fine-tune them.

The two parameterizations represent fundamentally different approaches to modeling urban effects on the mesoscale. In the W-UCM all urban effects are considered to be subgrid scale in the vertical, such that all urban processes are assumed to occur below the lowest model sigma level. Hence, the W-UCM is considered a single-layer parameterization. However, the W-UCM parameterizes in a fairly sophisticated manner a wide range of urban processes (Kusaka and Kimura 2004a,b). It includes the influence of (i) street canyons parameterized to represent variations in urban geometry, (ii) building shadowing and radiation reflection, and (iii) roof, wall, and road heat fluxes based upon explicit thermodynamic equations (Kusaka et al. 2001). The wall and road fluxes are computed based on an "urban canopy" temperature and wind defined at a height of the roughness length plus zero plane displacement height (effectively 2 m for urbanized regions). The urban canopy temperature is calculated from Eqs. (A1)–(A6) and the urban canopy wind is calculated from (A7)–(A10) as described in appendix A.

In contrast, the BW-UCM is considered a multilevel parameterization in that urban effects are computed vertically throughout the urban canopy. Thus, the urban canopy friction source is represented via modified aerodynamic drag in the momentum equations. Likewise, the thermal effects of the urban region are included through a modified thermodynamic equation that considers the heat fluxes from rooftop, street, and building wall reflections. Trapping of radiation in street canyons is considered as a nonprognostic heating term in the urban region. The urban canopy is treated as a source of turbulence production to account for turbulence wake generation via a modified TKE equation. The addition of a rooftop surface energy equation enables the parameterization to exhibit a more reasonable diurnal cycle of the heat island effect (Chin et al. 2005; see appendix B). Because of the uncertainty in specification of the spatial and diurnal variability in anthropogenic heating, as well as its impacts for urban regions (Sailor and Lu 2004), and to focus on fundamental differences in the two parameterizations, the anthropogenic heating is assumed to be zero for both parameterizations. Model statistics and validation for the two parameterizations will use the W-UCM urban canopy and BW-UCM 2-m air temperatures (computed from 10-m values based on Monin–Obukhov similarity theory) and the W-UCM urban canopy and 10-m BW-UCM wind components.

Urban parameterizations require several input parameters to describe the morphology of the urban environment. For this study a combination of the USGS 24-category 1-km dataset and a gridded 250-m resolution database for Manhattan (Burian et al. 2005) is used. The most important urban parameter is the determination of urban versus nonurban regions. For nests 4 and 5 of both simulations, Manhattan urban regions are determined using the Burian et al. (2005) dataset and for all other regions the USGS dataset is used, with only regions designated as urban utilizing the urban parameterization. Figure 2 shows the predominant land-use categories for each grid box for COAMPS nest 5. The majority of the nonurban land-use areas are grassland [i.e., approximately 61% for the

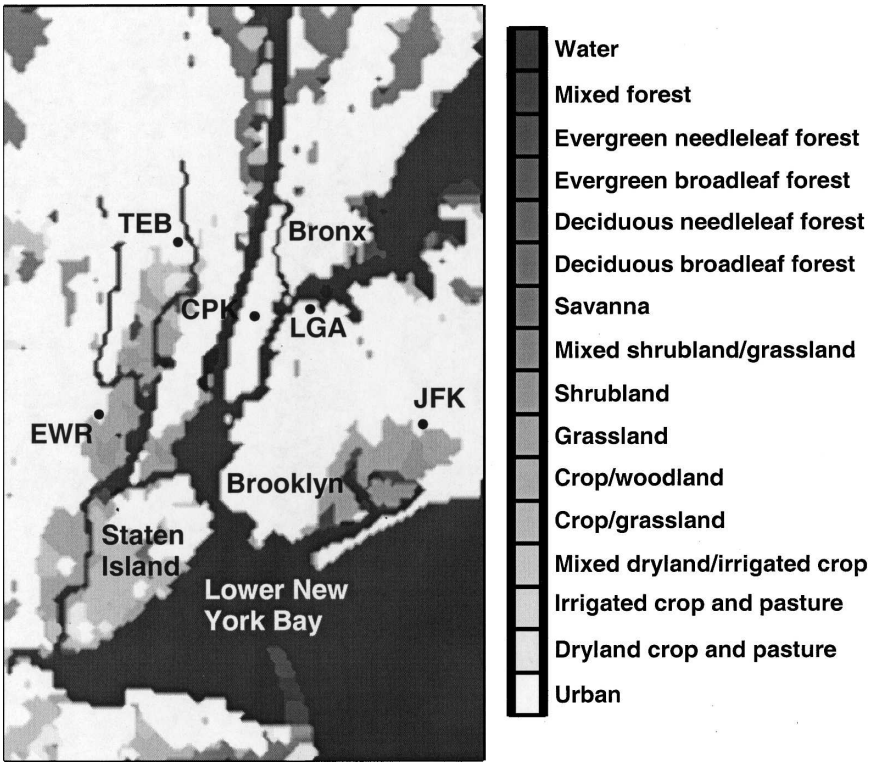

FIG. 2. COAMPS nest 5 (0.444 km) predominant land-use categories for each grid box along with points of interest discussed in the text.

region south of the John F. Kennedy Airport (JFK) and 54% for the region from Newark, New Jersey (EWR), to Teterboro, New Jersey (TEB), or crop/grassland (i.e., 51% for Staten Island)]. Manhattan is designated as high-intensity residential land-use land cover (LULC) type, and other suburban regions are designated as low-intensity residential LULC.

An important urban parameter is the building or urban canopy height. For urban regions outside of Manhattan, the default value of 10 m is used for BW-UCM, meaning that the urban canopy is similarly contained within the model's lowest sigma level for both W-UCM and BW-UCM. Over Manhattan, the 250-m database is used, with the tallest buildings generally concentrated in midtown and lower Manhattan with the maximum building height at approximately 200 m (Fig. 3). The 250-m database also provides urban plan area fraction used to determine roof and urban fractions. For W-UCM the building height must be less than the lowest model level plus the displacement height and are assigned values of 7.5 and 5.0 m (Manhattan and the suburbs; see Table A1).

To effectively simulate the surface fluxes in an urban environment, the urban parameterization should be coupled to the LSM to account for urban–vegetative effects. The urban–LSM coupling used here is based on an "urban percentage" to represent the subgrid-scale variability (Chen et al. 2004b; Kimura 1989). The Noah LSM calculates surface fluxes from natural or vegetated urban areas such as parks, trees, lawns, etc., and the urban parameterization calculates fluxes for man-made or artificial surfaces such as roads and buildings. The total grid-scale flux F_{tot} is a combination of the two, accounting for the fractional area coverage of vegetation versus artificial surfaces for a grid box (as determined from Burian et al. 2005):

$$F_{\text{tot}} = f_{\text{urb}} \times F_{\text{urb}} + f_{\text{nat}} \times F_{\text{LSM}}, \quad (1)$$

where f_{urb} is the urban grid fraction, f_{nat} is the natural fraction ($=1 - f_{\text{urb}}$), F_{urb} is the urban flux, and F_{LSM} is the natural flux. [In the appendixes, Tables A1 and A2 summarize the W-UCM urban parameters and Tables B1 and B2 summarize the BW-UCM parameters used in COAMPS for nests 4 and 5 derived from Burian et al. (2005) and Brown and Williams (1998).]

3. Model evaluation and statistical analysis

Model simulations of the 23-day period in August 2005 are evaluated against the Meteorological Aviation Report (METAR) near-surface observations and sta-

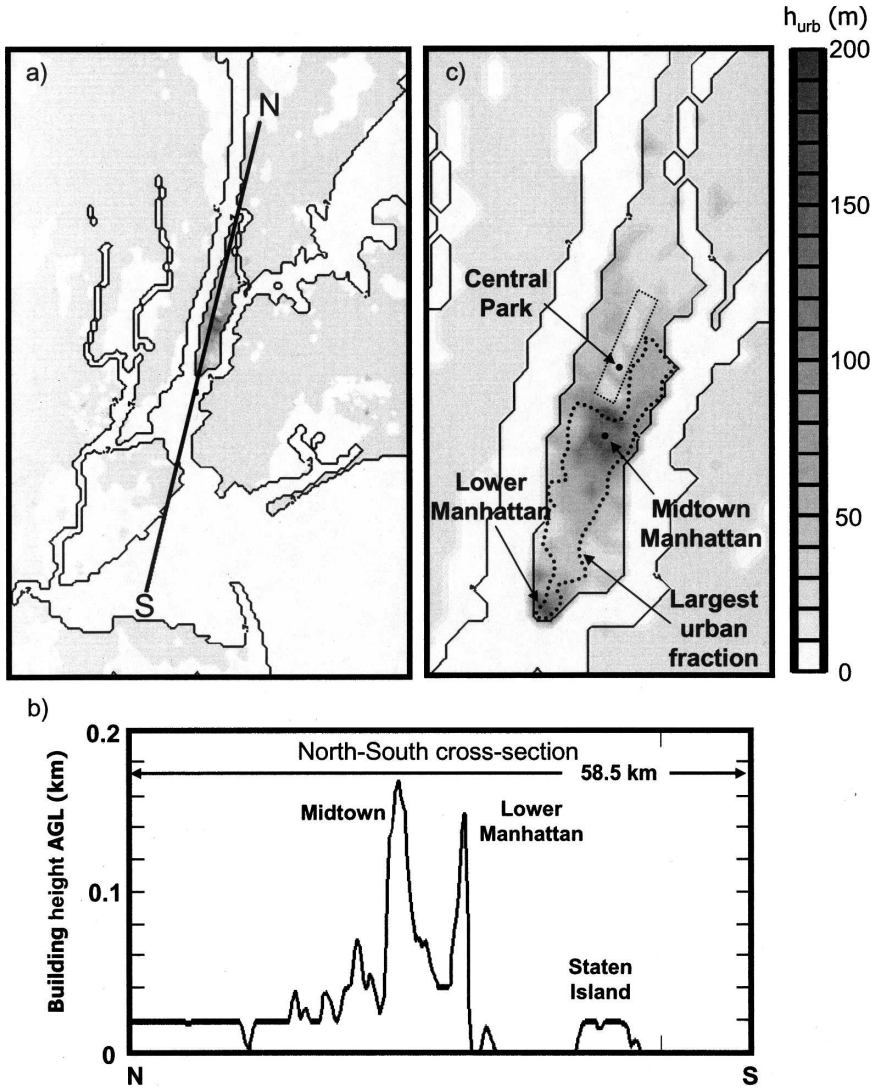

FIG. 3. (a) COAMPS nest 5 (0.444 km) building heights (m) used in the urban parameterization, (b) building heights along cross section N–S, and (c) subset of COAMPS nest 5 (0.444 km) building heights (m) showing regions of tallest buildings (shaded darker) and largest urban fraction (>0.8; enclosed in dotted line).

tistics are computed and compared for the two simulations. Figure 4 shows the time series of sea level pressure observed at three of the stations in the NYC metropolitan area along with time periods of measurable precipitation. The period from 5 to 27 August over the northeastern United States is characterized by varying synoptic and mesoscale forcing. During the period there were four cold frontal passages (6, 15, 18, and 22 August) and two periods dominated by quasi-stationary fronts (12 and 20 August). Measurable precipitation occurred on 7 days (8, 13, 15, 16, 17, 19, and 21 August), with observations in Brooklyn, New York, recording the lowest total rainfall for the month of August (0.17 in.) since records began in 1950. Observations in the Bronx, New York, recorded 2.83 in. for the month, with 2.62 in. occurring on 15 August (the evening of 14 August to the early morning of 15 August), a record rainfall for the date.

The time period from 1200 UTC 12 August to 0000 UTC 15 August 2005 was a particularly active period for storms, with several severe thunderstorm warnings issued by the National Weather Service (NWS) Storm Prediction Center, and will be discussed in more detail in section 4. On 12 August an approaching cold front dominated the New England states (Fig. 5). Strong surface daytime heating was evident along the prefrontal surface trough just west of the NYC area of eastern Pennsylvania and northern New Jersey. Near-surface

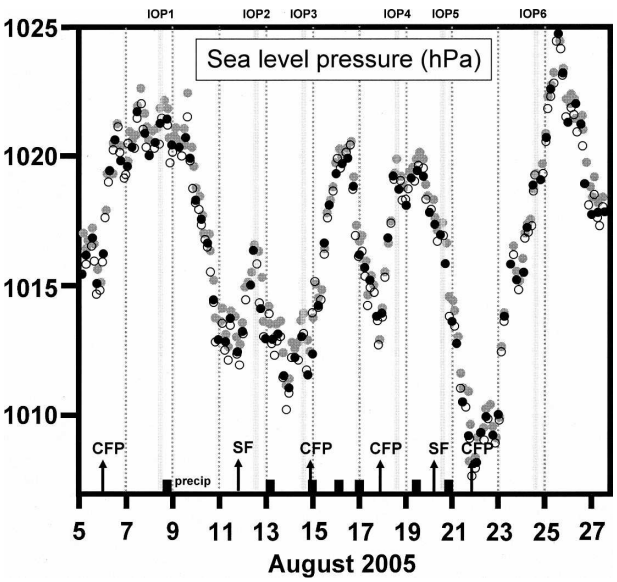

FIG. 4. Time series of observed sea level pressure (hPa) at EWR (black dots), LGA (open dots), and JFK (gray dots) Airports from 5 to 27 Aug 2005. The IOPs are indicated by the vertical shaded regions and time periods of measurable precipitation (from NWS observers at Bronx and Brooklyn) are indicated by small solid rectangles along the abscissa. Cold frontal passages (CFPs) and stationary front (SF) time periods are indicated by the vertical arrows.

temperatures exceeded 32°C (90°F), with dewpoints as large as 21°C (70°F) in the warm sector. Midlevel convective available potential energy approached 3000 J kg^{-1} and convective development was evident in satellite imagery as the front merges with the prefrontal trough by 2100 UTC. By 0000 UTC 13 August the front had moved northward into central New York and northern Connecticut with southerly flow over NYC and strong convection developing over the metropolitan area (Fig. 5b). As the front pushed to the north, NYC remained in the warm sector for much of 13 August, with a shortwave trough developing from southern New York and stretching southwestward into central North Carolina. Thunderstorms were observed in advance of the cold front over eastern Pennsylvania in the late afternoon on 13 August and into the early morning on 14 August (figure not shown). The front became quasistationary by 1200 UTC 14 August, aligned approximately southeast–northwest through north-central Pennsylvania into central Massachusetts. Multicell and supercell structures occured in the warm, moist sector with thunderstorms reported over the NYC metropolitan area in the late afternoon on 14 August, with record rainfall for the Bronx.

Mean observed and modeled statistics computed for the 23-day period at five METAR stations in the NYC metropolitan area for urban canopy air temperature, dewpoint depression, and wind speed are shown in Tables 1, 2, and 3, respectively. Each of the five stations is characterized as urban as shown in Fig. 2. Mean air temperatures are generally cold for both simulations compared with observations, with the exception of W-UCM at JFK and CPK (Table 1). However, the average mean bias for all five stations is significantly reduced using W-UCM, with an average of −0.10°C for W-UCM versus −0.82°C for BW-UCM. Likewise there is less variability using W-UCM, with an average rmse of 1.96° versus 2.37°C for BW-UCM. For dewpoint depression (Table 2) BW-UCM is generally drier than W-UCM (average mean bias of 0.35°C versus −0.02°C) and slightly more variable (average mean rmse of 3.26° versus 3.20°C) with Newark showing the largest reduction in rmse error. Mean wind speeds are light for all stations (less than 3 m s^{-1}; Table 3). BW-UCM typically overestimates speeds (average mean bias of 0.49 m s^{-1}) and W-UCM somewhat underestimates (−0.05 m s^{-1}). Stations at La Guardia Airport (LGA) and JFK have the biggest reduction in mean wind speed bias. There is significantly less variability in wind speed for W-UCM (average mean rmse of 0.91 m s^{-1}) than BW-UCM (1.17 m s^{-1}).

The cooler mean temperature bias for both simulations is due primarily to an underestimation of the nighttime air temperatures. Figure 6 shows the time series of observed and simulated wind speed, air temperature, and dewpoint depression along with the differences (model − observations) for EWR, considered representative of the stations in the metropolitan area (based on similar mean bias and rmse as compared to the average for all stations). The largest negative air temperature differences (model colder than observations) are primarily at night (maximum of −5.5°C for W-UCM at 0000 UTC 14 August and −6.2°C for BW-UCM at 0100 UTC 24 August). The largest differences between the two simulations in air temperature also occur at night and are most prominent during two time periods labeled A (6–12 August) and E (22–27 August) in Fig. 6. Both of these time periods are post–cold frontal when air temperatures are typically cooler than the climatological average for the metropolitan area. During these periods the nighttime temperatures for BW-UCM are as much as 3°–4°C colder than W-UCM. There is less difference in the daytime maximum temperatures between the two simulations. The largest daytime biases typically occur immediately following frontal passage (periods A, 1700 UTC 6 August, and C, 1700 UTC 15 August) in which both have difficulties in predicting cloud cover and overestimate the daytime heating. The dewpoint depression differences show that

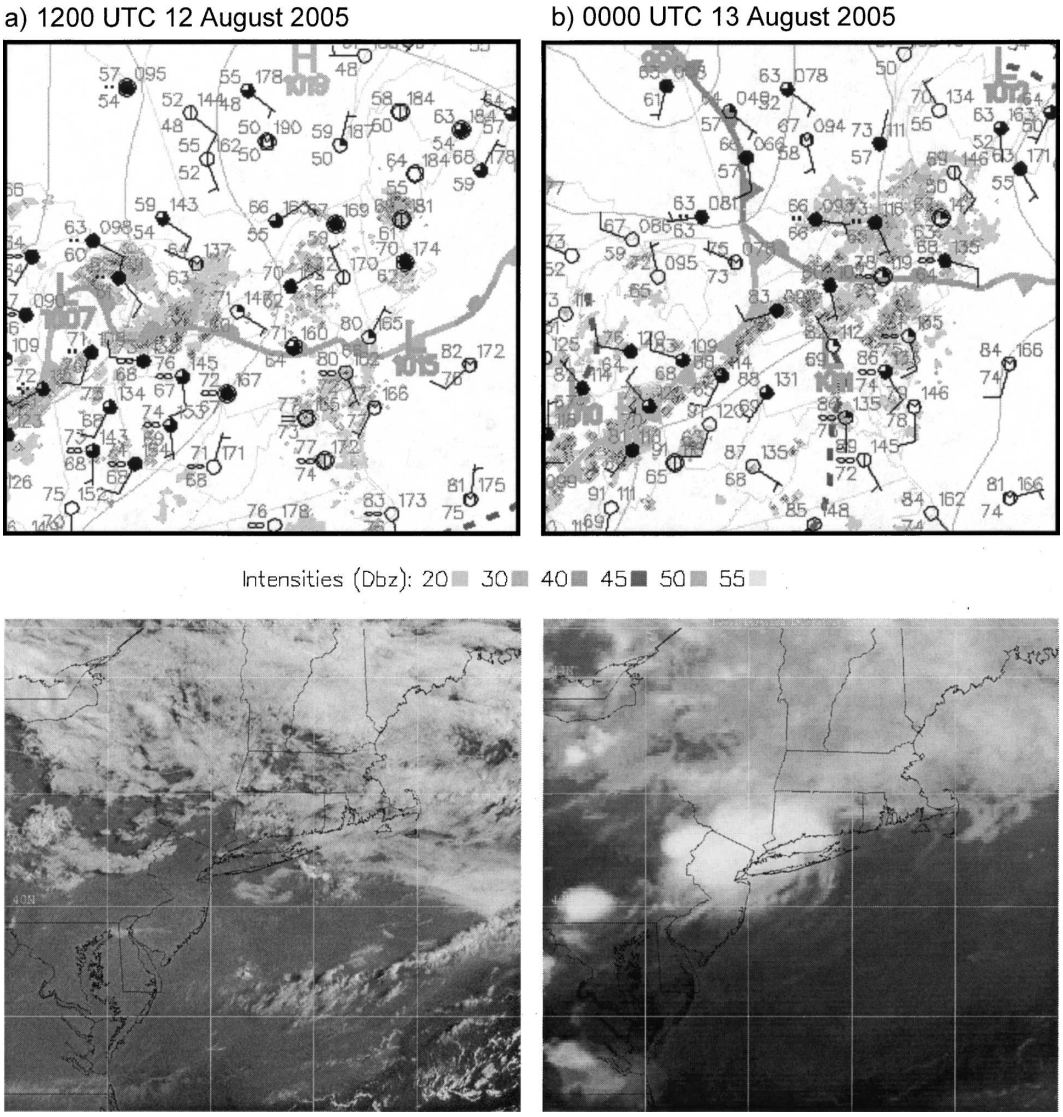

FIG. 5. (top) Surface analysis and (bottom) *GOES-12* satellite image valid at (a) 1200 UTC 12 Aug 2005 and (b) 0000 UTC 13 Aug 2005.

these time periods are ones in which both simulations are much too dry during the daytime (depression differences >10°C on 6 August and >5°C on 15 August). During the high heat period following the warm frontal passage (time period B) both simulations more accurately predict the maximum daytime temperatures (bias approximately 1°C) than the nighttime (bias approximately −3°C), and likewise show the largest moist bias at night for the 23-day period (<−6°C). Overall, the wind speeds for both simulations show similar temporal characteristics with no discernible correlation to frontal passage, but there is more of a tendency for BW-UCM to overestimate speeds during the daytime as compared with W-UCM. This feature is most prominent at JFK as seen in the much larger mean bias (2.99 m s^{-1}) in Table 3.

Differences in mean fields over the diurnal cycle are examined for daytime (0800–2000 LT) and nighttime (2100–0700 LT) periods. Figure 7 shows the mean day and nighttime urban canopy temperatures for the two simulations and their differences. The W-UCM is generally warmer at daytime over much of the metropolitan area by approximately 1°C (Figs. 7a–c). Temperatures for regions southeast of EWR are similar for both simulations, but other areas are as much as 1.5°C warmer for the W-UCM (north of TEB). The daytime effect of the sea breeze on the coastal areas of Brooklyn and regions near JFK is more prominent in the W-

TABLE 1. Urban canopy air temperature statistics computed for observations at EWR, LGA, JFK, TEB, and at the Belvedere Castle in CPK and nest 5 model simulations for BW-UCM and W-UCM for the 0–12-h forecasts for the 23-day period from 0000 UTC 5 Aug to 1200 UTC 27 Aug 2005. (a) Mean and standard deviations and (b) mean bias (model − observation), rmse, and correlation coefficient.

Urban canopy air temperature (°C)	No. obs	Mean	Std dev
	EWR		
Obs	540	26.22	3.93
BW-UCM	540	25.18	5.04
W-UCM	540	25.98	4.45
	LGA		
Obs	540	26.45	3.36
BW-UCM	540	25.15	4.46
W-UCM	540	25.74	4.14
	JFK		
Obs	540	25.09	3.27
BW-UCM	540	24.55	3.98
W-UCM	540	25.37	3.59
	TEB		
Obs	540	25.85	4.01
BW-UCM	540	25.17	4.89
W-UCM	540	25.79	4.65
	CPK		
Obs	540	25.59	3.62
BW-UCM	540	25.05	4.61
W-UCM	540	25.82	4.14

Urban canopy air temperature (°C)	Mean bias	RMSE	Correlation coef
	EWR		
BW-UCM	−1.04	2.73	0.87
W-UCM	−0.24	2.01	0.89
	LGA		
BW-UCM	−1.30	2.73	0.85
W-UCM	−0.71	2.28	0.85
	JFK		
BW-UCM	−0.54	1.88	0.89
W-UCM	0.28	1.54	0.91
	TEB		
BW-UCM	−0.68	2.15	0.91
W-UCM	−0.06	1.95	0.91
	CPK		
BW-UCM	−0.54	2.38	0.87
W-UCM	0.23	2.02	0.88

TABLE 2. Urban canopy dewpoint depression statistics computed for observations at airports at EWR, LGA, and JFK and nest 5 model simulations for BW-UCM and W-UCM for the 0–12-h forecasts for the 23-day period from 0000 UTC 5 Aug to 1200 UTC 27 Aug 2005 similar to Table 1.

Urban canopy dewpoint depression (°C)	No. obs	Mean	Std dev
	EWR		
Obs	540	9.22	5.13
BW-UCM	540	9.67	6.02
W-UCM	540	9.26	5.85
	LGA		
Obs	540	8.94	4.16
BW-UCM	540	8.76	5.44
W-UCM	540	8.61	5.61
	JFK		
Obs	540	6.85	4.64
BW-UCM	540	7.65	4.78
W-UCM	540	7.09	4.70

Urban canopy dewpoint depression (°C)	Mean bias	RMSE	Correlation coef
	EWR		
BW-UCM	0.45	3.42	0.83
W-UCM	0.04	3.23	0.83
	LGA		
BW-UCM	−0.18	3.29	0.80
W-UCM	−0.33	3.34	0.81
	JFK		
BW-UCM	0.79	3.06	0.80
W-UCM	0.24	3.02	0.79

UCM. The increase in the mean dewpoint (figure not shown) is larger for the W-UCM for these regions (generally by 3°–5°C) because of the sea breeze. The horizontal temperature gradient from JFK to LGA is 0.15°C km^{-1} for W-UCM compared with only 0.08°C km^{-1} for the BW-UCM. At night the suburban areas for the BW-UCM cool much more than for the W-UCM. The mean temperatures for W-UCM are generally warmer than the BW-UCM over much of the metropolitan area by approximately 1°C (Figs. 7d–f). The strength of the UHI is estimated using an urban location in Manhattan and a rural location in the northwest corner of nest 5 (marked by an asterisk in Fig. 7a). The maximum strength is 12.2°C at 2000 UTC 25 August for the W-UCM but only 5.4°C for BW-UCM at 2300 UTC 14 August. In the mean the UHI is stronger for the W-UCM, averaging 2.2° versus 1.9°C for the BW-UCM. Gedzelman et al. (2003) found a typical UHI effect of 4°C using an "urban" average of four airport stations scattered across the region and a "rural" average of four sites located 50 km inland. The rural site used here is ~20 km northwest of Manhattan, so the calculations have a smaller footprint in terms of spatial coverage. Also, the occurrence of sea breezes during the simulations presented here can create surface inversions that may reduce the UHI (Bornstein 1968).

Figure 8 shows the day and nighttime mean urban canopy winds and differences for the two simulations. The strong southerly component of the sea breeze is the dominant wind feature during the daytime. Over water, wind speeds are generally largest south of JFK (6–7 m s^{-1}) for both simulations. There is significant flow acceleration from Lower New York Bay through the Verrazano Narrows into Upper New York Bay. Daytime winds over much of Brooklyn north to almost LGA are generally stronger for W-UCM than for BW-

TABLE 3. Urban canopy wind speed statistics computed for observations at airports at EWR, LGA, JFK and nest 5 model simulations for BW-UCM and W-UCM for the 0–12-h forecasts for the 23-day period from 0000 UTC 5 Aug to 1200 UTC 27 Aug 2005 similar to Table 2.

Urban canopy wind speed ($m\ s^{-1}$)	No. obs	Mean	Std dev
	EWR		
Obs	540	1.98	0.85
BW-UCM	540	2.17	0.99
W-UCM	540	1.78	0.79
	LGA		
Obs	540	2.02	0.86
BW-UCM	540	2.47	1.06
W-UCM	540	2.08	0.90
	JFK		
Obs	540	2.16	1.00
BW-UCM	540	2.99	1.41
W-UCM	540	2.17	0.89
Urban canopy wind speed ($m\ s^{-1}$)	Mean bias	RMSE	Correlation coef
	EWR		
BW-UCM	0.19	0.98	0.46
W-UCM	−0.20	0.85	0.49
	LGA		
BW-UCM	0.45	1.09	0.47
W-UCM	0.06	0.94	0.42
	JFK		
BW-UCM	0.83	1.45	0.56
W-UCM	0.004	0.94	0.51

UCM (approximately 0.5–1.0 $m\ s^{-1}$ stronger) in association with the stronger inland penetration of the sea breeze, which is also evident in the mean temperatures (Fig. 7). Daytime winds over Manhattan are generally less for BW-UCM ($<1.5\ m\ s^{-1}$) compared with W-UCM ($2.0\ m\ s^{-1}$). At night the mean overwater wind direction for both simulations is southwesterly, with overland winds very light and variable. Again, the low wind speed signature over Manhattan is more prominent in BW-UCM than W-UCM.

Figures 9 and 10 show subsets of nest 5 centered over Manhattan of urban canopy temperatures and winds, respectively, overlaid with regions of maximum building height and urban fraction. The temperatures and winds for BW-UCM are more closely correlated with the urban fraction than W-UCM as expected based upon the BW-UCM equations (see appendix B). The mean day and nighttime temperatures for both simulations show warmer temperatures over lower Manhattan south of CPK (the region of highest urban fraction) and cooler temperatures over CPK and to the north (the lower urban fraction; Fig. 9). Overall, though, both the day and nighttime mean temperatures over lower Manhattan for the W-UCM are approximately 1°C warmer than the BW-UCM. CPK shows much stronger nighttime cooling for the BW-UCM and is approximately 1.5°C cooler than the W-UCM. There is much less dependence of temperature differences on urban characteristics but more dependence on land surface characteristics.

The decrease in urban wind speed is most prominent for the BW-UCM both day and nighttime over lower Manhattan (Fig. 10). The daytime decrease is generally over the region of tallest building heights (winds $<1\ m\ s^{-1}$), while the nighttime decrease extends over much of lower Manhattan and appears influenced by both building height as well as urban fraction (Fig. 10e). In contrast, the daytime winds for the W-UCM show little horizontal variation over Manhattan (Fig. 10a). The nighttime winds show a decrease in speed similar to the BW-UCM but over a much smaller area confined to the high urban fraction region between lower Manhattan and midtown. The daytime wind differences correlate closely with regions of the tallest buildings with mean differences as large as $2\ m\ s^{-1}$. Nighttime differences are similarly located but smaller in magnitude (approximately $1\ m\ s^{-1}$). The day and nighttime mean winds over CPK and the less urbanized regions to the north show little differences. Thus, there is much more dependence of wind differences on urban characteristics and less on land surface characteristics.

The mean daytime urban canopy dewpoint depression over Manhattan (figure not shown) is similar for both simulations (approximately 12°–14°C) with little horizontal variation. However, the nighttime mean values are more strongly influenced by urban variations. Both simulations show the largest depressions (driest conditions) for lower Manhattan (BW-UCM approximately 7°C versus 5.5°–6°C for W-UCM) and moister conditions for CPK (BW-UCM approximately 6° versus 5°C for W-UCM). The mean day and nighttime surface fluxes of latent heat (figure not shown) are typically less than $5\ W\ m^{-2}$ for both simulations for all of Manhattan with the exception of CPK (approximately 25–50 $W\ m^{-2}$). The mean sensible heat flux is more closely correlated to the urban characteristics than the latent flux. The largest urban fraction regions of lower Manhattan (typically the warmest regions) also have the largest mean flux. Values for BW-UCM are less than W-UCM both at daytime (approximately 150 versus $200\ W\ m^{-2}$) and nighttime (approximately 10 versus $15\ W\ m^{-2}$).

4. Model simulations for high heat day (12 August 2005)

The two model simulations are examined in greater detail for the 24-h time period from 0000 UTC 12 August during the Intensive Observing Period (IOP) 2 of

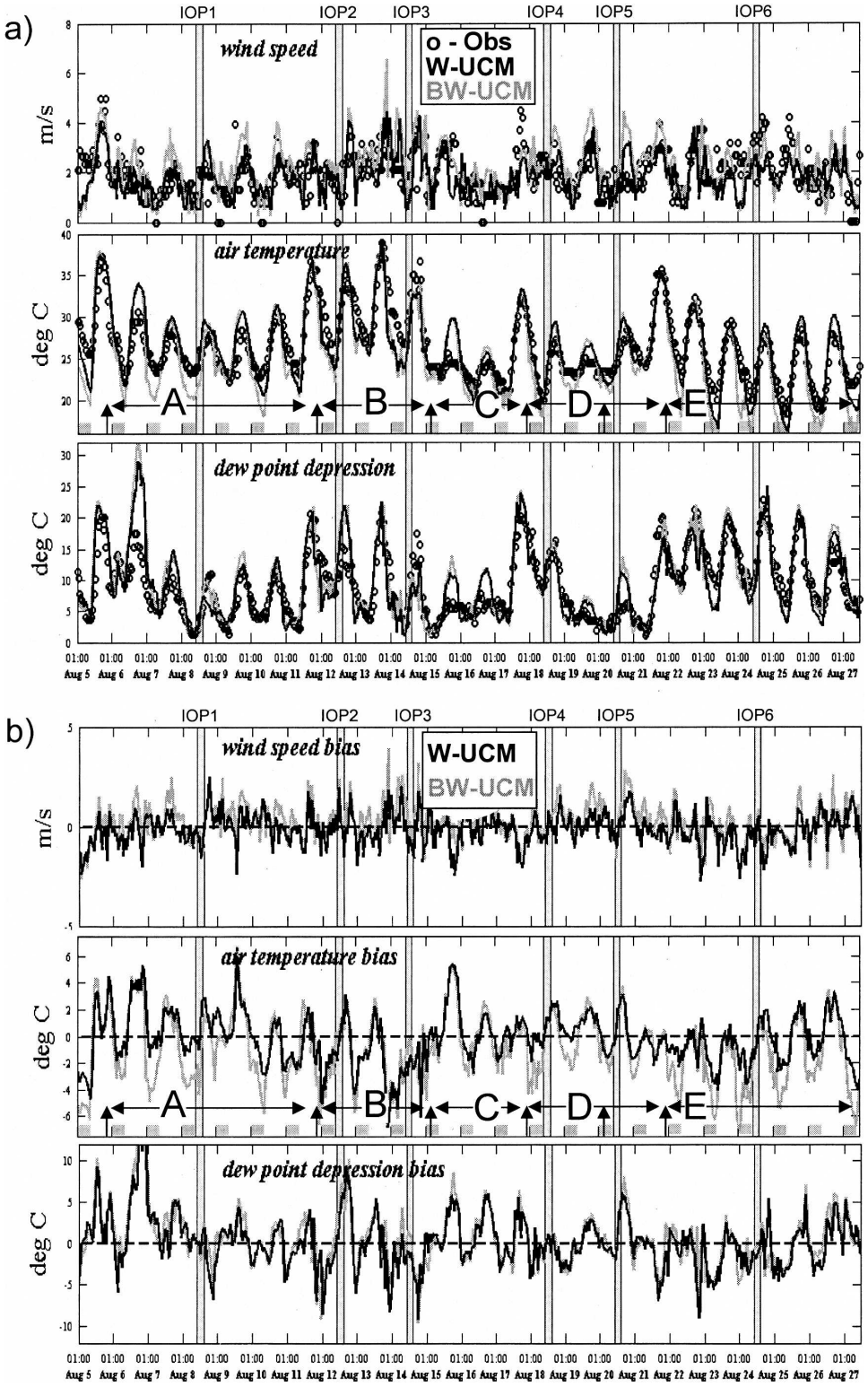

FIG. 6. (a) Time series at EWR of observations (open circles) and COAMPS simulations W-UCM (black) and BW-UCM (gray) for urban canopy wind speeds (m s^{-1}), air temperature (°C), and dewpoint depression (°C) and (b) the difference (model − observation). The nighttime periods are indicated by the shaded gray rectangles along the abscissa. The six IOPs are indicated by the shaded vertical lines and the vertical arrows indicate frontal passages as in Fig. 4. The time periods designated A to E are discussed in the text.

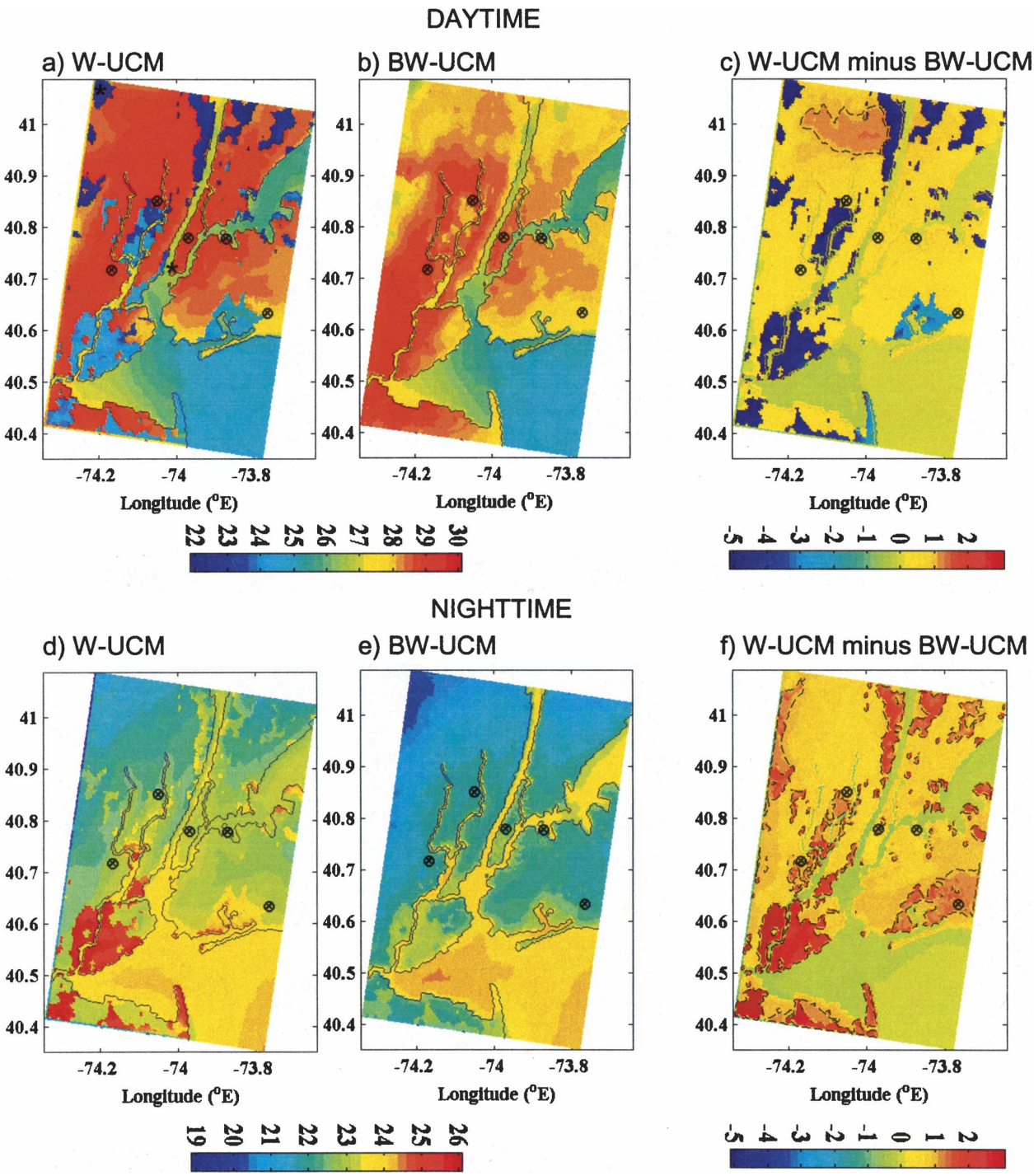

FIG. 7. Mean urban canopy air temperature (°C) for daytime for (a) W-UCM, (b) BW-UCM, and (c) W-UCM minus BW-UCM, and nighttime for (d) W-UCM, (e) W-UCM, and (f) W-UCM minus BW-UCM for the 23-day period from 5 to 27 Aug 2005. The contour of 1°C is shown for the difference plots. The locations of the validation points are given by the circles and the asterisks in (a) indicate locations used to compute UHI values.

the field program. This time period proved particularly challenging to produce accurate wind forecasts needed by the field personnel in preparation for tracer release. As discussed in the previous section, on this day there is a warm frontal passage in conjunction with an afternoon sea breeze with a shift of low-level winds from northeasterly to south-southeasterly with near–record high temperatures.

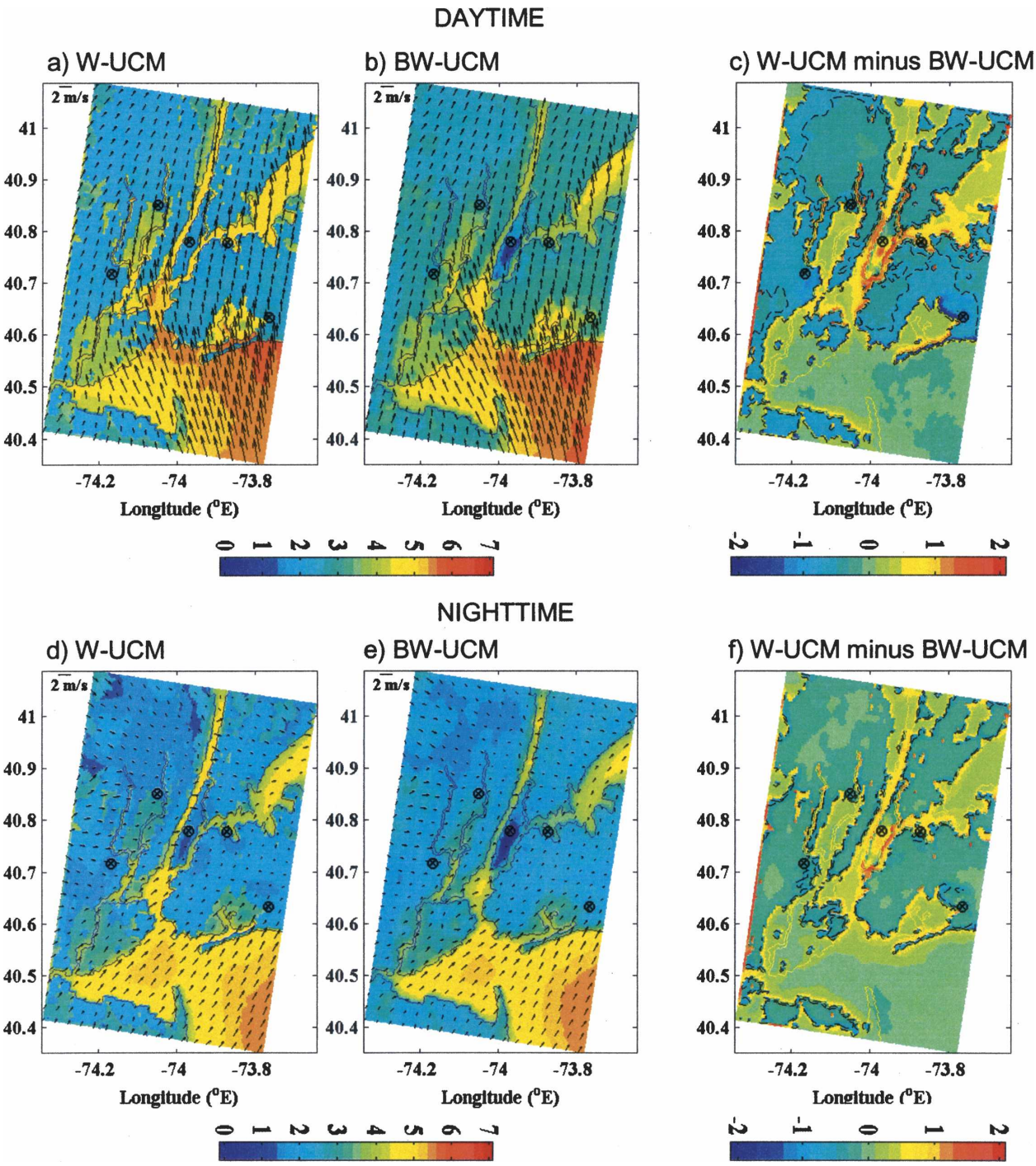

FIG. 8. Mean urban canopy wind ($m\ s^{-1}$) for daytime for (a) W-UCM, (b) BW-UCM, (c) W-UCM minus BW-UCM, and nighttime for (d) W-UCM, (e) BW-UCM, and (f) W-UCM minus BW-UCM similar to Fig. 7. Every sixth wind arrow is plotted and the contour shown for differences is 0.5 $m\ s^{-1}$.

Figure 11 shows the urban canopy air temperature and winds for the BW-UCM simulation for 1500, 1800, and 2100 UTC 12 August illustrating the penetration of the sea-breeze front into the metropolitan area. The general evolution of the sea-breeze fronts discussed here for the BW-UCM applies also to the W-UCM simulation (figure not shown), though the strength of the sea-breeze front is slightly larger than the BW-UCM. At 1500 UTC (1100 LT) the sea breeze has just begun to form along virtually all of the coastal regions

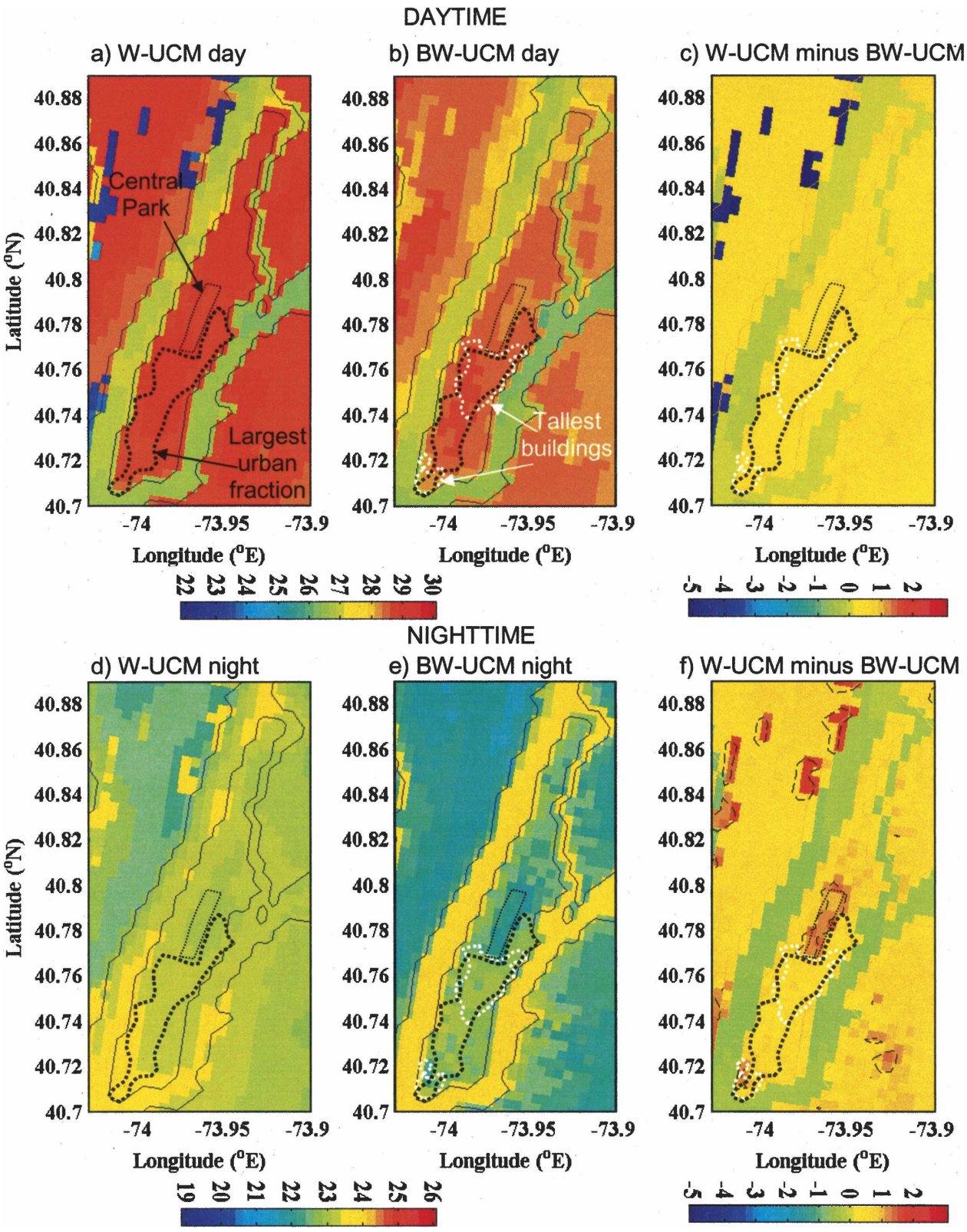

FIG. 9. Mean urban canopy air temperature (°C) for the subset of nest 5 over Manhattan for daytime for (a) W-UCM, (b) BW-UCM, (c) W-UCM minus BW-UCM, and nighttime for (d) W-UCM, (e) BW-UCM, and (f) W-UCM minus BW-UCM. The heavy dotted black line indicates the regions of largest urban fraction (>0.8) and the heavy dotted white line indicates the regions of tallest buildings (>75 m) as determined from Burian et al. (2005). The light dotted black line indicates CPK.

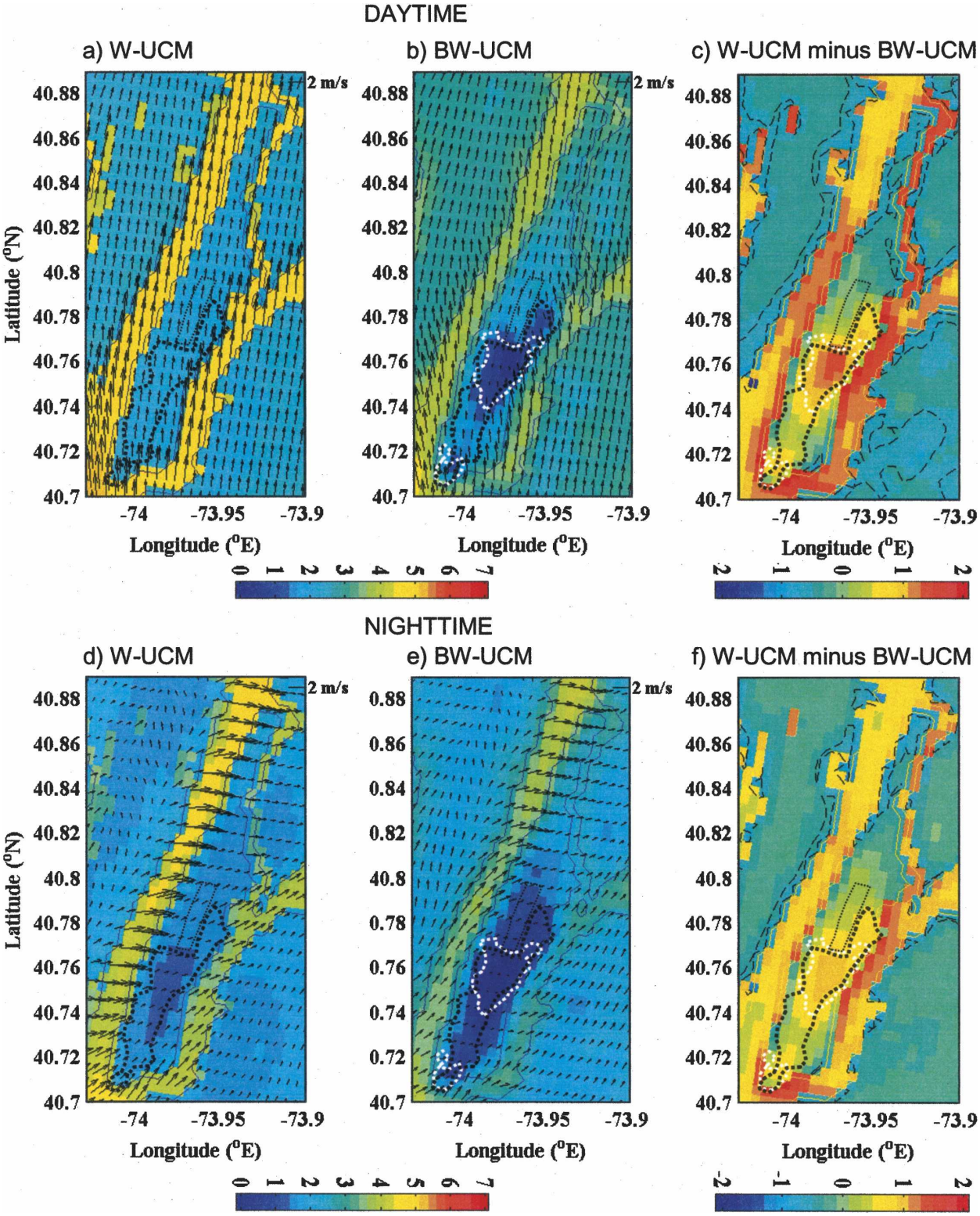

FIG. 10. Mean urban canopy wind ($m\,s^{-1}$) for a subset of nest 5 over Manhattan for daytime for (a) W-UCM, (b) BW-UCM, (c) W-UCM minus BW-UCM, and nighttime for (d) W-UCM, (e) BW-UCM, and (f) W-UCM minus BW-UCM similar to Fig. 9. Wind arrows are shown for every grid point in the east–west direction and every other grid point in the north–south direction.

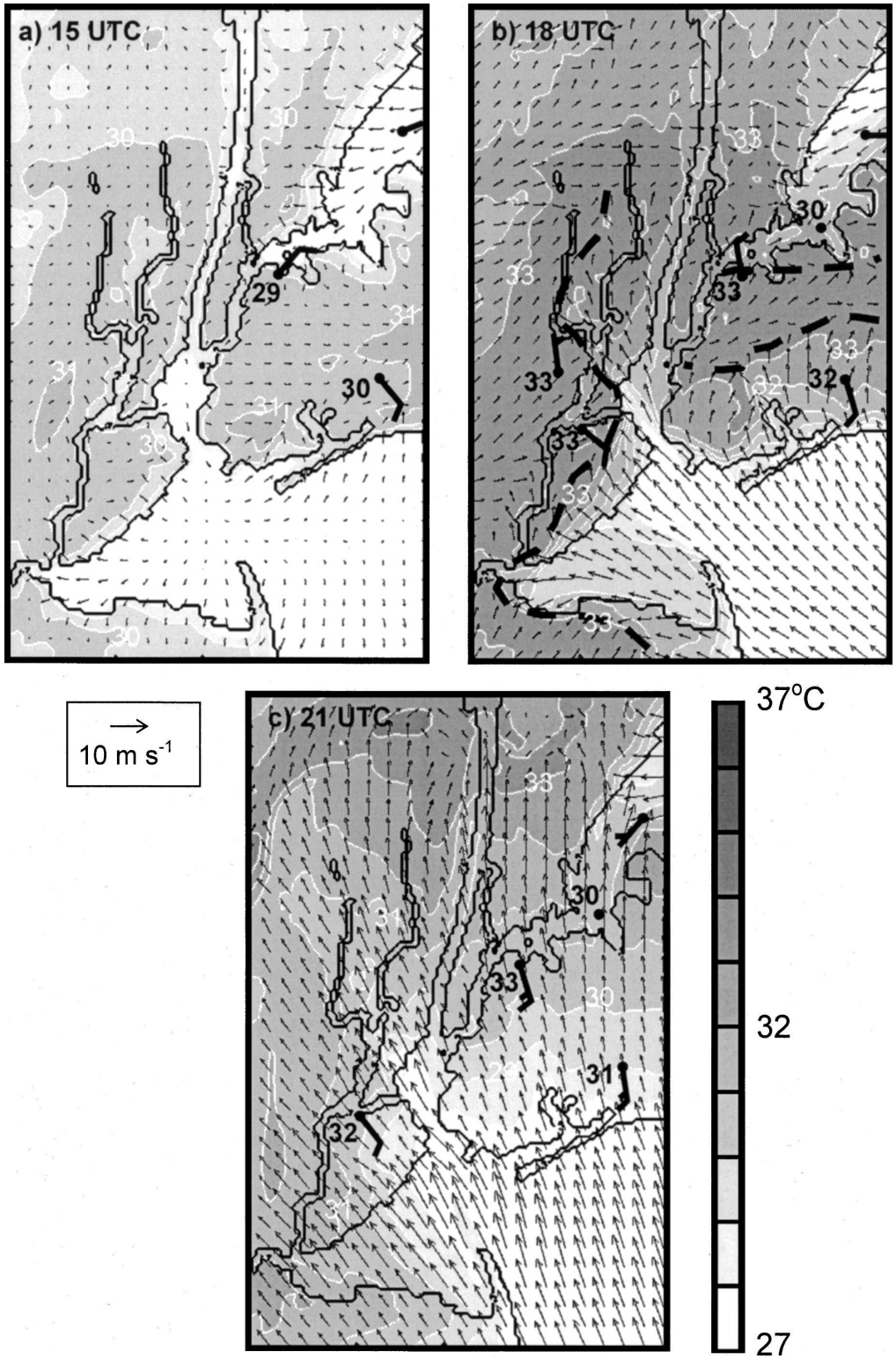

FIG. 11. COAMPS nest 5 (0.444 km) BW-UCM simulation of urban canopy temperatures (shaded, interval = 1°C) and winds (arrows, every fifth grid point) valid at (a) 1500, (b) 1800, and (c) 2100 UTC 12 Aug 2005. Observations are plotted in black (temperature, °C; winds full barb = 5 m s^{-1}). The subjective location of the sea-breeze front at 1800 UTC based on the model forecast is given by the heavy dashed line.

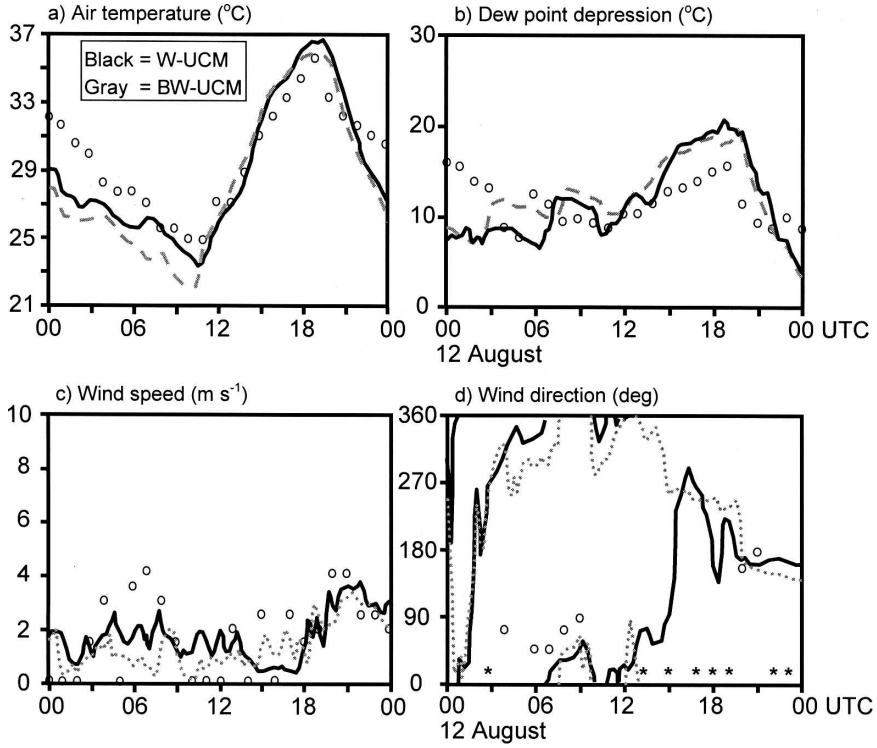

FIG. 12. Time series at CPK from 0000 UTC 12 Aug to 0000 UTC 13 Aug 2005 of (a) air temperature (°C), (b) dewpoint depression (°C), (c) wind speed (m s^{-1}), and (d) wind direction (°). The nest 5 COAMPS simulations are two 12-h forecasts for W-UCM (black) and BW-UCM (gray). The solid line represents the W-UCM urban canopy values, the dashed line represents the 2-m BW-UCM values, and the dotted line represents the 10-m wind values. The open circles are the observations and the asterisks along the abscissa for wind direction indicated periods in which the observed wind direction was reported as variable.

in the metropolitan area, including both the southern and northern shores of Long Island, along Staten Island, and the Hudson and East Rivers as well as Long Island Sound (Fig. 11a). This common occurrence of multiple sea-breeze boundaries is supported by observations in the metropolitan area (Novak and Colle 2006; Colle et al. 2003). The front is very weak but onshore flow is evident in the simulation as well as observed at LGA and JFK. By 1800 UTC (1400 LT) the frontal boundaries are well defined, as indicated in the model by the dashed lines as well as the observations (Fig. 11b). However, over Manhattan the front is less easily identified. Thompson et al. (2007) show additional evidence of the difficulty of identifying the sea-breeze front as it propagates across Manhattan.

Figure 12 shows the time series at CPK of temperature, dewpoint depression, and winds for the 24-h period. Observations indicate that the sea-breeze front does not definitively reach CPK until 2000 UTC. At that time the winds shift to southerly and increase to approximately 4 m s^{-1} (along with a decrease in dewpoint depression) though winds are variable and increase to ~3 m s^{-1} as early as 1500 UTC in conjunction with a wind shift to southerly in both simulations. Both simulations characterize CPK as an urban surface, but one dominated by vegetation with low urban fraction (<0.05) and low building heights (~10 m). Thus, features forced by surface fluxes will be influenced more directly by vegetated land surface effects than urban effects [based upon the partitioning given in Eq. (1)].

The minimum and maximum observed temperatures for 12 August are 25.0° (at 1100 UTC) and 35.6°C (at 1900 UTC; Fig. 12a; range of 10.6°C). The nighttime cold bias for BW-UCM is approximately 1°C larger than for W-UCM, with both simulations similar for the daytime maximum. The nighttime cold bias is significantly improved for W-UCM urban canopy temperatures (black solid line) due to wall and road effects in W-UCM (as evident in the mean temperatures shown in Fig. 9). Contrast that to the nighttime temperatures at a more urbanized site in midtown Manhattan characterized by higher urbanization (fraction > 0.8) and

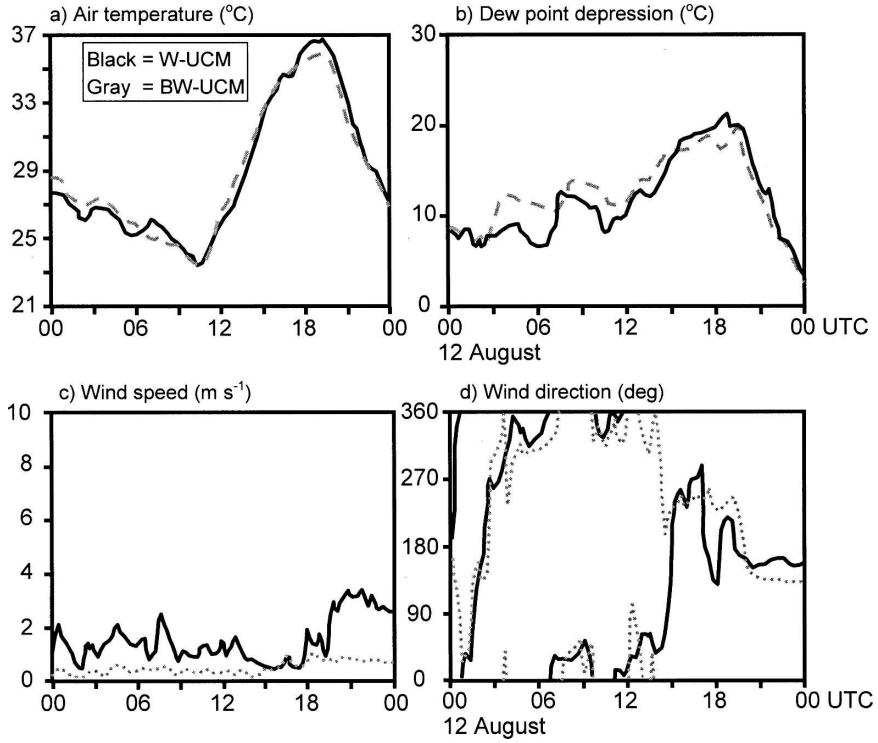

FIG. 13. Time series at midtown Manhattan from 0000 UTC 12 Aug to 0000 UTC 13 Aug 2005 of (a) air temperature (°C), (b) dewpoint depression (°C), (c) wind speed (m s^{-1}), and (d) wind direction (°). The nest 5 COAMPS simulations are two 12-h forecasts for W-UCM (black) and BW-UCM (gray). The solid line represents the urban canopy values for W-UCM, the dotted line represents the 10-m values, and the dashed line represents the 2-m values similar to Fig. 12. Unfortunately no observations are available at this site.

taller buildings (>125 m; Fig. 13). The nighttime BW-UCM 2-m temperatures are more than 2°C warmer than at CPK and agree well with W-UCM. This further emphasizes the greater sensitivity of BW-UCM to the specification of urbanization. W-UCM shows fewer differences from site CPK to midtown, supporting the conclusions evident in the mean values (Fig. 9).

For the 24-h period there are fewer differences in dewpoint depression with both simulations overpredicting at daytime (too dry by approximately 3°–4°C; Figs. 12b and 13b). This is in contrast to the mean in which CPK typically has smaller depressions. The observed winds are light (<2–3 m s^{-1}) from the northeast for most of the night and early afternoon until the seabreeze front passes and the speeds increase to ~4 m s^{-1}. Winds for both simulations show good agreement with observations at CPK (Figs. 12c,d). The 10-m BW-UCM wind speeds are most strongly affected by the urbanization (Fig. 13c), with speeds generally less than 1 m s^{-1}, a factor of 3–4 less than W-UCM (as seen in the mean fields shown in Fig. 10).

The urban effects at midtown Manhattan are also evident in the development of the nocturnal heat island. Low-level time–height cross sections of the gradient Richardson number (Ri) illustrate the more strongly stable nocturnal surface layer that sets up over the urban regions in BW-UCM as compared to W-UCM (Fig. 14). A strong surface-based stable layer (Ri > 0.25) extending to approximately 50–75 m AGL is present from 0000 to 1100 UTC undercutting the overlying residual layer for BW-UCM. In contrast, a neutral layer exists in the W-UCM simulation, forming by 0300 UTC up to 50 m AGL and deepening to ~150 m by 0800 UTC. The more strongly stable nighttime surface layer in BW-UCM also impacts the amount of TKE generated near the surface (Fig. 15). Note that there is very little nighttime TKE for BW-UCM at either CPK or midtown (average <0.1 $m^2 s^{-2}$). In contrast W-UCM nighttime values are much larger, particularly at midtown where the urban effects are largest (average of approximately 0.7 $m^2 s^{-2}$). During the daytime both simulations show similar TKE profiles at CPK where urban effects are less significant, but daytime BW-UCM TKE at midtown is actually less than CPK due to the large reduction in wind speed (and vertical shear) associated with the tall buildings.

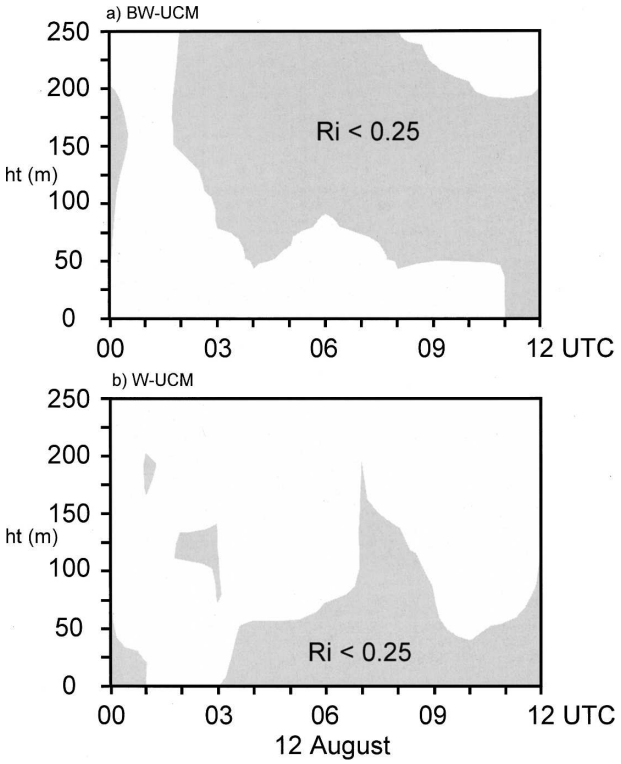

FIG. 14. Nighttime time–height cross section of gradient Ri at the midtown Manhattan site from 0000 to 1200 UTC 12 Aug 2005 for (a) BW-UCM and (b) W-UCM. The shaded regions represent areas where the Ri is less than 0.25.

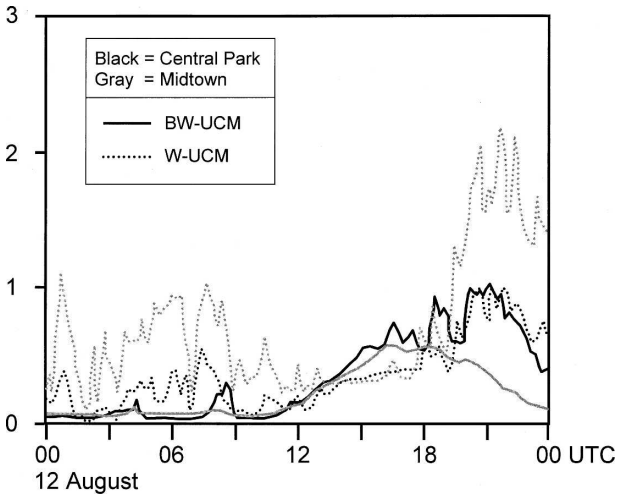

FIG. 15. Diurnal variations in urban canopy turbulent kinetic energy ($m^2 s^{-2}$) from 0000 UTC 12 Aug to 0000 UTC 13 Aug 2005 for CPK (black lines) and midtown Manhattan (gray lines). The solid lines represent the BW-UCM simulation and the dotted lines represent the W-UCM simulation.

This reduction dominates the explicit increase in TKE production in the BW-UCM parameterization [Eq. (A14)].

Figure 16 shows the CPK and midtown Manhattan diurnal energy balances at the reference 10-m height representing the total energy heat budget of the two simulations. In both simulations the latent heat flux is less at midtown by a factor of 2 compared with CPK, as expected because of the urban surfaces. The W-UCM ground heat flux for midtown is much larger during the daytime than the BW-UCM (peak of approximately 300 versus 100 W m^{-2}; Fig. 16b), and effectively shifts the period of positive sensible flux later into the early evening. This helps to maintain the near-surface mixed layer at night in the W-UCM simulation and produces the nocturnal heat island (Kusaka and Kimura 2004b). Observations have shown that this heating during the several hours after sunset is important for the development of the UHI (Grimmond and Oke 1995). This supports the much stronger UHI for the W-UCM compared with the BW-UCM discussed in section 3 and evident in the mean day–night temperature fields (Fig. 9). The W-UCM ground heat flux is also a much larger negative flux just after sunset compared with the BW-UCM. This feature is similar to single-column simulations by Kusaka et al. (2001) who attributed it to the large effective thermal inertial of the urban surface. This is supported by the fact that the more vegetated CPK region has significantly smaller ground heat flux (Fig. 16a).

The diurnal variations in the W-UCM roof, wall, and road temperatures emphasize the effect of the urban structures on the maintenance of the UHI (Fig. 17). The roof temperature shows the largest diurnal amplitude (30.9°C), which is 2.7°C larger than the road temperature amplitude. This result is consistent with the results of Kusaka et al. (2001) and Kusaka and Kimura (2004a) who also used the W-UCM parameterization but in a 2D study. The reason is that the road surface temperature remains higher after sunset due to the smaller sky view factor and larger volumetric heat capacity. The wall surface temperature cooling rate is much smaller than that for the roof and road surfaces, resulting in the walls being the warmest surface at night (by ~1°–2.5°C). Kusaka and Kimura (2004b) hypothesized that this feature is an important one for the maintenance of the nocturnal heat island.

5. Summary and conclusions

A high-resolution modeling study has been designed to realistically represent aspects of the mesoscale circulation in the NYC metropolitan area. To that end, we have included parameterizations of the urban canopy using a high-resolution building database and supplied hourly high-fidelity ocean model–derived SSTs on the innermost two nests of the COAMPS model domain (1.33- and 0.44-km resolution). We evaluate the effects

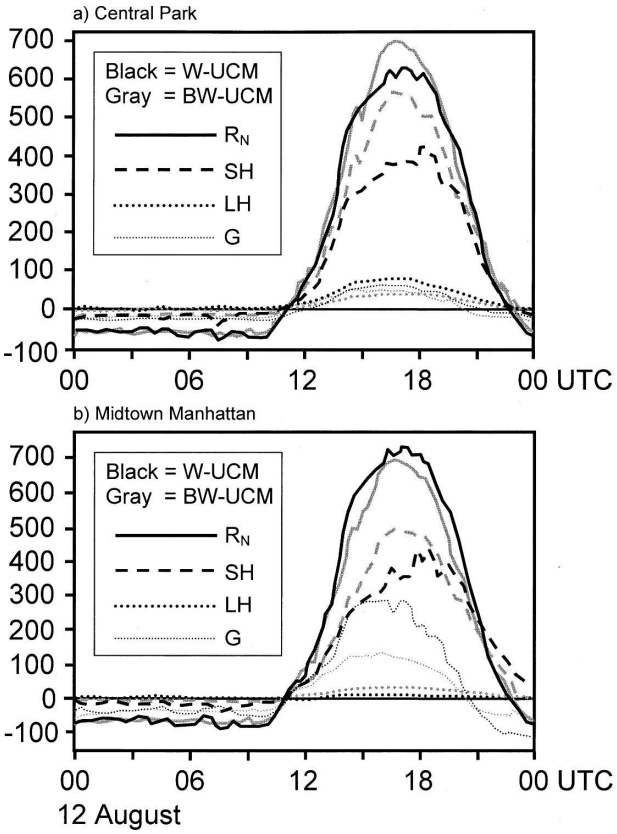

FIG. 16. Diurnal energy balances (W m^{-2}) from 0000 UTC 12 Aug to 0000 UTC 13 Aug 2005 for (a) CPK and (b) midtown Manhattan. The black lines represent the W-UCM simulation and the gray lines represent the BW-UCM simulation. The solid, dashed, dotted, and thin dotted lines are the net radiation, sensible heat flux, latent heat flux, and ground heat flux, respectively.

of two differing urban parameterizations for simulations during an extended period (5–27 August 2005) of the NYC UDP field campaign, and in depth for a case study of a high heat day with sea-breeze penetration into the metropolitan area.

The two parameterizations have been widely used in the modeling community and represent fundamentally different approaches to modeling urban effects on the mesoscale. The single-layer W-UCM is the recently installed urban model for the WRF community model and the multilayer BW-UCM has been tested for a variety of different case study simulations in the U.S. Navy mesoscale model COAMPS. These simulations are conducted using the default values for the parameterizations and no attempt has been made to optimize or fine-tune the parameterizations. The purpose is to assess the new initial WRF urban capability versus a multilevel parameterization for long-term simulations. As such this is the first comparison of these parameterizations over several weeks for real-data simulations at high resolution.

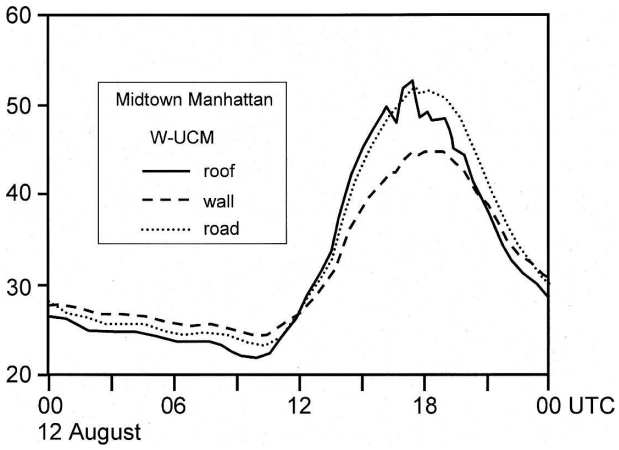

FIG. 17. Diurnal variations in surface temperatures (°C) from 0000 UTC 12 Aug to 0000 UTC 13 Aug 2005 for midtown Manhattan. The solid, dashed, and dotted lines represent the W-UCM temperatures of rooftop, wall, and road, respectively.

The period from 5 to 27 August 2005 exhibited four cold frontal passages through the NYC metropolitan area, two prominent quasi-stationary fronts, and 7 days with measurable precipitation. Mean statistics computed for the 23-day period show a cold mean urban canopy air temperature bias due primarily to an underestimation of nighttime temperatures in both simulations. The largest air temperature differences between the two simulations occur during post–cold frontal time periods when temperatures are typically cooler than the climatological average for the metropolitan area. During these periods the nighttime temperatures for the BW-UCM are as much as 3°–4°C colder than the W-UCM. The daytime biases are generally smaller than nighttime and typically occur immediately following frontal passage when both simulations have difficulties in predicting cloud cover and overestimate the daytime heating. Overall, the mean temperature bias is significantly reduced using W-UCM (−0.10°C for the W-UCM versus −0.82°C for the BW-UCM) due to the development of a stronger nocturnal UHI (mean value of 2.2°C for the W-UCM versus 1.9°C for the BW-UCM).

Results from a 24-h case study during a high heat day with inland sea-breeze penetration (12 August 2005) indicate W-UCM better maintains the UHI through increased nocturnal warming due to wall and road effects. The ground heat flux for W-UCM is much larger during the daytime than BW-UCM (peak of approximately 300 versus 100 W m^{-2}), effectively shifting the period of positive sensible flux later into the early evening. This helps to maintain the near-surface mixed layer at night in the W-UCM simulation and sustains the nocturnal UHI. In contrast, the BW-UCM simulation develops a strong surface-based nocturnal stable layer extending

approximately 50–75 m deep. Subsequently, the nocturnal BW-UCM wind speeds are a factor of 3–4 less than the W-UCM with reduced nighttime turbulent kinetic energy (average $< 0.1\ \mathrm{m^2\ s^{-2}}$).

The implementation of the multilayer BW-UCM parameterization imposes greater dependence on the characterization of urbanization characteristics such as building heights and roof fractions than does the single-layer W-UCM parameterization. For the densely urbanized area of Manhattan, the BW-UCM winds show more dependence on urbanization than the W-UCM. The decrease in urban wind speed is most prominent for the BW-UCM both day and nighttime over lower Manhattan, with the daytime decrease generally over the region of tallest building heights while the nighttime decrease is influenced by both building height as well as urban fraction. In contrast, the W-UCM winds show less horizontal variation over Manhattan, particularly during the daytime.

This result stresses the need for ongoing research that is focused on improving our understanding of the sensitivity of urban parameterizations to the specification of the urban morphology within the model. Kusaka et al. (2001) note that their scheme is sensitive to building height and that less is known about how tall buildings impact the urban temperature structure. Preliminary offline COAMPS W-UCM simulations for a single cold start forecast (initialized from global 1° fields) at 0000 UTC 12 August examined the sensitivity to increasing building heights over Manhattan (up to 30 m). The results suggest that there is more sensitivity at night versus day to such changes in depth. As the depth of the urban canopy increases, the nocturnal surface layer warms much more than the daytime layer. The impacts of diurnal variability of anthropogenic heat flux as stressed by Sailor and Lu (2004) is also another important area in which our understanding is limited. As more high-resolution urban databases are made available, more in-depth verification and validation of such urban processes in these parameterizations is needed. Subsequent intelligent optimization and tuning of the parameterizations can be expected.

Acknowledgments. We are grateful to Mukul Tewari and Fei Chen of the National Center for Atmospheric Research for providing the W-UCM code, Steve Burian of the University of Utah for assembling the New York–New Jersey building database, Alan Blumberg of Stevens Institute of Technology for making available the NYHOPS SSTs, and Dan Kohn for processing some of the observations. We benefited from discussions with Hiroyuki Kusaka, William Thompson, Michael Brown, and Brian Colle. This work was supported by the DHS UDP through Grants P4CF40592 and P5CH40318.

APPENDIX A

Description of the W-UCM Urban Parameterization

The W-UCM is based on the single-layer urban canopy parameterization of Kusaka et al. (2001). The model computes surface temperatures of roof, wall, and road from the surface energy balance:

$$R_{N,i} = \mathrm{SH}_i + \mathrm{LH}_i + G_i, \tag{A1}$$

where R_N is the net downward radiative flux, SH is the sensible heat flux, LH is the latent heat flux, and G is the ground heat flux, for surfaces i (roof, road, or wall). Sensible heat flux from the wall ($\mathrm{SH_{wall}}$) and road ($\mathrm{SH_{road}}$) are calculated using Jurges's formula (Tanaka et al. 1993):

$$\mathrm{SH_{wall}} = C_w(T_w - T_s), \tag{A2}$$

$$\mathrm{SH_{road}} = C_{\mathrm{road}}(T_{\mathrm{road}} - T_s), \tag{A3}$$

where

$$\begin{aligned} C_w = C_{\mathrm{road}} &= 7.51U_s^{0.78} \quad \text{for} \quad U_s > 5\ \mathrm{m\ s^{-1}} \\ &= 6.15 + 4.18U_s \quad \text{for} \quad U_s \le 5\ \mathrm{m\ s^{-1}}, \end{aligned} \tag{A4}$$

where T_w and T_{road} are wall and road surface temperatures, respectively; T_s is the "urban canopy" temperature at the height of the thermal roughness length z_T plus the zero plane displacement height d; and U_s is the wind speed at the height of the momentum roughness length plus d. The sensible heat flux between the canopy and the overlying atmosphere is computed as

$$\mathrm{SH} = \rho c_p \frac{ku_*}{\Psi_h}(T_s - T_a), \tag{A5}$$

where ρ is air density, c_p is specific heat of dry air, u_* is friction velocity, T_a is air temperature at a reference height (10 m), and Ψ_h is a universal stability function:

$$\Psi_h = \int_{\zeta_T}^{\zeta} \frac{\phi_h}{\zeta'}\, d\zeta', \tag{A6}$$

where $\zeta_T = z_T/L$ and $\zeta = (z_a - d)/L$, with L the Monin–Obukhov length.

The urban canopy wind speed U_s is computed using the wind profile equation of Swaid (1993):

$$U_s = U_r \exp\left(-0.386\frac{h}{w}\right), \tag{A7}$$

TABLE A1. Parameters for COAMPS W-UCM simulations for nests 4 and 5 urban regions.

	Manhattan	Suburban regions
Urban fraction	Burian et al. (2005)	0.2
Building height (m)	7.5	5.0
Momentum roughness length above canyon (m)	0.75	0.5
Heat roughness length above canyon (m)	0.75	0.5
Zero plane displacement height (m)	1.5	1.0
Momentum roughness length above canyon	5.0	0.2
Sky view factor	0.56	0.62
Building drag coef	0.2	0.2
Building volumetric parameter (m^{-1})	0.4	0.3

TABLE A2. Parameters for COAMPS W-UCM simulations for nests 4 and 5 urban regions.

	Value
Heat capacity of roof, building, and walls (cal cm^{-3} K^{-1})	0.5
Thermal conductivity of roof, building, and walls (cal cm^{-1} s^{-1} K^{-1})	0.004
Albedo of roof, building, and walls	0.15
Emissivity of roof, building, and walls	0.97
Momentum roughness length of roof, building, and walls (m)	0.1
Heat roughness length of roof, building, and walls (m)	0.01
No. of layers of roof, building, and walls	4

where h is the normalized building height, w is the normalized road width, and U_r is the wind speed at roof level given as

$$U_r = U_a \frac{\Psi_{mr}}{\Psi_m}, \tag{A8}$$

where U_a is the wind speed at the reference height (10 m), and Ψ are universal stability functions:

$$\Psi_m = \int_{\zeta_o}^{\zeta} \frac{\phi_m}{\zeta'} d\zeta', \tag{A9}$$

$$\Psi_{mr} = \int_{\zeta_o}^{\zeta_r} \frac{\phi_m}{\zeta'} d\zeta', \tag{A10}$$

where $\zeta_r = (h_{\text{urb}} - d)/L$, with h_{urb} being the building height.

The individual wall, roof, and road temperatures are calculated as balanced temperatures based on the surface heat fluxes. The one-dimensional energy conservation equation is numerically solved for the interior temperatures for the layers of the grid. The boundary condition is set as zero heat flux through the bottom layer. The ground heat flux $G_{z,i}$ and interior temperature $T_{z,i}$ at a depth z for surface i (wall, roof, and road) are computed as

$$G_{z,i} = -\lambda_i \frac{\partial T_{z,i}}{\partial z}, \tag{A11}$$

$$\frac{\partial T_{z,i}}{\partial t} = -\frac{1}{\rho_i c_i} \frac{\partial G_{z,i}}{\partial z}, \tag{A12}$$

where λ_i is the interior thermal conductivity and $\rho_i c_i$ is the volumetric heat capacity.

The radiative effects of building shadowing and reflection are discussed in detail in Kusaka et al. (2001). The model parameters used in Tables A1 and A2 are the default values similar to Kusaka et al. (2001, their Tables III and IV).

APPENDIX B

Description of the BW-UCM Urban Parameterization

The BW-UCM is a multilayer model based on Brown and Williams (1998) extended from Yamada (1982) and modified by Chin et al. (2005). Model predictive equations are modified to include contributions from urban effects. The urban canopy acts as a friction source in the momentum equations:

$$\frac{\partial U}{\partial t} = \ldots - f_{\text{roof}} C_d a(z) U|U|, \tag{B1}$$

$$\frac{\partial V}{\partial t} = \ldots - f_{\text{roof}} C_d a(z) V|V|, \quad \text{and} \tag{B2}$$

$$\frac{\partial W}{\partial t} = \ldots - f_{\text{roof}} C_d a(z) W|W|, \tag{B3}$$

where U, V, and W are wind components, f_{roof} is the horizontal roof fraction, C_d is the drag coefficient of the urban canopy, and $a(z)$ is the building surface area density profile assumed to decrease linearly from the surface (=1) to 0 at the top of the building (Chin et al. 2005). The urban canopy also acts as a turbulence source in the turbulence kinetic energy (q^2) equation:

$$\frac{\partial q^2}{\partial t} = \ldots + f_{\text{roof}} C_d a(z)(|U|^3 + |V|^3 + |W|^3). \tag{B4}$$

The impact of urban effects on temperature is given in the potential temperature (Θ) equation:

TABLE B1. Urban parameters for COAMPS BW-UCM simulations for nests 4 and 5 separated by region.

	Building height (m)	Urban fraction	Roof fraction	Urban drag (N m^{-2})
Manhattan	Burian et al. (2005) See Fig. 3	Burian et al. (2005)	Burian et al. (2005)	Building height × 0.0005
Suburban regions	10	0.2	0.1	0.01

$$\frac{\partial \Theta}{\partial t} = \ldots + (\pi \rho c_p)^{-1}\left\{(1 - f_{\text{urb}})\frac{\partial R_N}{\partial z} + f_{\text{urb}}\frac{\partial q_{\text{urb}}}{\partial z} + (1 + B^{-1})^{-1}\left[(f_{\text{urb}} - f_{\text{roof}})\frac{\partial R_{NC}}{\partial z} + f_{\text{roof}} b(z) C_{\text{roof}}^{-1} \rho c_p \Delta q_{\text{roof}}\right]\right\}, \tag{B5}$$

where R_{NC} is the net downward radiative flux for street canyon regions of the urban canopy defined as

$$R_{NC}(z) = R_h^{\text{net}\downarrow} \exp[-kL(z)], \tag{B6}$$

where $R_h^{\text{net}\downarrow}$ is the net downward total radiative flux at the top of the urban canopy, k is the radiative extinction coefficient, and $L(z)$ is the cumulative index of the building surface area calculated as

$$L(z) = \int_z^{h_{\text{urb}}} a(z)\, dz, \tag{B7}$$

where h_{urb} is the height of the urban canopy, R_N is the net downward radiative flux in the nonurban regions, π is the nondimensional pressure, ρ is the air density, c_p is the specific heat of dry air at constant pressure, f_{urb} is the urban fraction, q_{urb} is the anthropogenic heat flux, B is the Bowen ratio of the urban canopy, C_{roof} is the roof heat capacity, Δq_{roof} is the heat flux change of the rooftop surface, and $b(z)$ is the normalized roof surface area density function defined at each vertical k level as

$$b(z_k) = \frac{a(z_k)dz_k}{\Sigma a(z_k)dz_k}, \tag{B8}$$

where dz_k is the vertical depth within the urban canopy, and

$$\Delta q_{\text{roof}} = R_{\text{SW}}^{\downarrow}(1 - \alpha) + \varepsilon(R_{\text{LW}}^{\downarrow} - \sigma T^4) - \rho c_p C_{\text{d\_roof}} |V|(T_{\text{roof}} - T), \tag{B9}$$

TABLE B2. Urban parameters for COAMPS BW-UCM simulations for nests 4 and 5.

Parameter	Value
Roof emissivity	0.91
Roof drag coef	0.0071
Radiative extinction coef	0.1
Bowen ratio	1.5
Roof albedo	0.22
Roof heat capacity	1.38×10^5 J m^{-2} K^{-1}

where $R_{\text{SW}}^{\downarrow}$ and $R_{\text{LW}}^{\downarrow}$ are the downward shortwave and longwave radiative fluxes at the rooftop, α is the roof albedo, ε is the roof emissivity, $C_{\text{d\_roof}}$ is the roof drag coefficient, V is the wind velocity, and T is the air temperature, where T_{roof} is computed from the rooftop surface energy equation:

$$\frac{\partial T_{\text{roof}}}{\partial t} = \frac{\Delta q_{\text{roof}}}{C_{\text{roof}}}. \tag{B10}$$

The urban effects on the surface energy budget are computed as

$$R_{NG} = (1 - f_{\text{urb}})(R_{\text{SW}}^{\text{net}\downarrow} - R_{\text{LW}}^{\text{net}\uparrow})_G + (f_{\text{urb}} - f_{\text{roof}})R_{NC}(\text{sfc}), \tag{B11}$$

where R_{NG} is the surface net total radiative flux. The model parameters used in Tables B1 and B2 are similar to those given in Chin et al. (2005).

REFERENCES

Avissar, R., and R. A. Pielke, 1989: A parameterization of heterogeneous land surfaces for atmospheric numerical models and its impact on regional meteorology. *Mon. Wea. Rev.,* **117,** 2113–2136.

Blumberg, A. F., and G. L. Mellor, 1987: A description of a three-dimensional coastal ocean circulation model. *Three-Dimensional Coastal Ocean Models,* N. S. Heaps, Ed., Amer. Geophys. Union, 1–16.

Bornstein, R. D., 1968: Observations of the urban heat island effect in New York City. *J. Appl. Meteor.,* **7,** 575–582.

——, and W. T. Thompson, 1981: Effects of frictionally retarded sea breeze and synoptic frontal passages on sulfur dioxide concentrations in New York City. *J. Appl. Meteor.,* **20,** 843–858.

——, and M. LeRoy, 1990: Urban barrier effects on convective and frontal thunderstorms. *Extended Abstracts, Fourth Conf. on Mesoscale Processes,* Boulder, CO, Amer. Meteor. Soc., 120–121.

Brown, M. J., and M. Williams, 1998: An urban canopy parameterization for mesoscale meteorological models. Preprints, *Second Symp. on the Urban Environment,* Albuquerque, NM, Amer. Meteor. Soc., 144–147.

Bruno, M. S., and A. F. Blumberg, 2004: An urban ocean obser-

vatory—Real-time assessments and forecasts of the New York Harbor marine environment. *Sea Technol.,* **45** (8), 27–32.

Burian, S. J., A. McKinnon, J. Hartman, and W. Han, 2005: National building statistics database: New York City. Los Alamos National Laboratory Final Rep. LA-UR-05-8154, National Building Statistics Database Project, 1 March 2005, 17 pp.

Ca, V. T., Y. Ashie, and T. Asaeda, 2002: A k-ϵ turbulence closure model for the atmospheric boundary layer including urban canopy. *Bound.-Layer Meteor.,* **102,** 459–490.

Chen, F., and J. Dudhia, 2001: Coupling an advanced land-surface/hydrology model with the Penn State/NCAR MM5 modeling system. Part I: Model implementation and sensitivity. *Mon. Wea. Rev.,* **129,** 569–585.

——, and Coauthors, 1996: Modeling of land-surface evaporation by four schemes and comparison with FIFE observations. *J. Geophys. Res.,* **101,** 7251–7268.

——, K. Manning, D. Yates, M. LeMone, S. Trier, R. Cuenca, and D. Niyogi, 2004a: Development of a High-Resolution Land Data Assimilation System (HRLDAS). Preprints, *16th Conf. on Numerical Weather Prediction,* Seattle, WA, Amer. Meteor. Soc., CD-ROM, 22.3.

——, H. Kusaka, M. Tewari, J.-W. Bao, and H. Hirakuchi, 2004b: Utilizing the coupled WRF/LSM urban modeling system with detailed urban classification to simulate the urban heat island phenomena over the greater Houston area. Preprints, *Fifth Conf. on Urban Environment,* Vancouver, BC, Canada, Amer. Meteor. Soc., CD-ROM, 9.11.

Chen, S., and Coauthors, 2003: COAMPS® version 3 model description. Naval Research Laboratory Publication NRL/PU/7500-03-448, Marine Meteorology Division, Monterey, CA, 143 pp.

Childs, P. P., and S. Raman, 2005: Observations and numerical simulations of urban heat island and sea breeze circulations over New York City. *Pure Appl. Geophys.,* **162,** 1955–1980.

Chin, H.-N. S., M. J. Leach, G. A. Sugiyama, J. M. Leone Jr., H. Walker, J. S. Nasstrom, and M. J. Brown, 2005: Evaluation of an urban canopy parameterization in a mesoscale model using VTMX and URBAN 2000 data. *Mon. Wea. Rev.,* **133,** 2043–2068.

Colle, B. A., J. B. Olson, and J. S. Tongue, 2003: Multi-season verification of the MM5. Part I: Comparison with the Eta model over the central and eastern United States and impact of MM5 resolution. *Wea. Forecasting,* **18,** 431–457.

Ek, M. B., K. E. Mitchell, Y. Lin, E. Rogers, P. Grunmann, V. Koren, G. Gayno, and J. D. Tarpley, 2003: Implementation of Noah land surface model advances in the National Centers for Environmental Prediction operational mesoscale Eta model. *J. Geophys. Res.,* **108,** 8851, doi:10.1029/2002JD003296.

Fan, S., A. Blumberg, M. Bruno, D. Kruger, and B. Fullerton, 2006: The skill of an urban ocean forecast system. *Proc. Ninth Int. Conf. on Estuarine and Coastal Modeling,* Charleston, SC, ASCE, 603–618.

Gedzelman, S. D., S. Austin, R. Cermak, N. Stefano, S. Partridge, S. Quesenberry, and D. A. Robinson, 2003: Mesoscale aspects of the urban heat island around New York City. *Theor. Appl. Climatol.,* **75,** 29–42.

Grimmond, C. S. B., and T. R. Oke, 1995: Comparison of heat fluxes from summertime observations in the suburbs of four North American cities. *J. Appl. Meteor.,* **34,** 873–889.

Grossman-Clarke, S., J. A. Zehnder, W. L. Stefanov, Y. Liu, and M. A. Zoldak, 2005: Urban modifications in a mesoscale meteorological model and the effects on near-surface variables in an arid metropolitan region. *J. Appl. Meteor.,* **44,** 1281–1297.

Harshvardhan, R. Davies, D. A. Randall, and T. G. Corsetti, 1987: A fast radiation parameterization for atmospheric circulation models. *J. Geophys. Res.,* **92,** 1009–1016.

Hodur, R. M., 1997: The Naval Research Laboratory's Coupled Ocean/Atmosphere Mesoscale Prediction System (COAMPS). *Mon. Wea. Rev.,* **125,** 1414–1430.

Holt, T. R., D. Niyogi, F. Chen, K. Manning, M. A. LeMone, and A. Qureshi, 2006: Effect of land–atmosphere interactions on the IHOP 24–25 May 2002 convection case. *Mon. Wea. Rev.,* **134,** 113–133.

Kain, J. S., and J. M. Fritsch, 1993: Convective parameterization for mesoscale models: The Kain–Fritsch scheme. *The Representation of Cumulus Convection in Numerical Models, Meteor. Monogr.,* No. 24, Amer. Meteor. Soc., 165–170.

Khairoutdinov, M., and Y. Kogan, 2000: A new cloud physics parameterization in a large eddy simulation model of marine stratocumulus. *Mon. Wea. Rev.,* **128,** 229–243.

Kimura, F., 1989: Heat flux on mixture of different land-use surface: Test of a new parameterization scheme. *J. Meteor. Soc. Japan,* **67,** 401–409.

Kusaka, H., and F. Kimura, 2004a: Thermal effects of urban canyon structure on the nocturnal heat island: Numerical experiment using a mesoscale model coupled with an urban canopy model. *J. Appl. Meteor.,* **43,** 1899–1910.

——, and ——, 2004b: Coupling a single-layer urban canopy model with a simple atmospheric model: Impact on urban heat island simulation for an idealized case. *J. Meteor. Soc. Japan,* **82,** 67–80.

——, H. Kondo, Y. Kikegawa, and F. Kimura, 2001: A simple single-layer urban canopy model for atmospheric models: Comparison with multi-layer and slab models. *Bound.-Layer Meteor.,* **101,** 329–358.

Liu, Y., F. Chen, T. Warner, and J. Basara, 2006: Verification of a mesoscale data-assimilation and forecasting system for the Oklahoma City area during the Joint Urban 2003 field project. *J. Appl. Meteor. Climatol.,* **45,** 912–929.

Loose, T., and R. D. Bornstein, 1977: Observations of mesoscale effects on frontal movement through an urban area. *Mon. Wea. Rev.,* **105,** 563–571.

Louis, J.-F., M. Tiedtke, and J. F. Geleyn, 1982: A short history of the operational PBL-parameterization of ECMWF. *Workshop on Planetary Boundary Layer Parameterization,* Reading, Berkshire, United Kingdom, European Centre for Medium-Range Weather Forecasts, 59–79.

Mahrt, L., and M. Ek, 1984: The influence of atmospheric stability on potential evaporation. *J. Climate Appl. Meteor.,* **23,** 222–234.

——, and H. L. Pan, 1984: A two-layer model of soil hydrology. *Bound.-Layer Meteor.,* **29,** 1–20.

Martilli, A., A. Clappier, and M. W. Rotach, 2002: An urban surface exchange parameterization for mesoscale models. *Bound.-Layer Meteor.,* **104,** 261–304.

Masson, V., 2000: A physically-based scheme for the urban energy budget in atmospheric models. *Bound.-Layer Meteor.,* **94,** 357–397.

Mellor, G. L., and T. Yamada, 1982: Development of a turbulence closure model for geophysical fluid problems. *Rev. Geophys.,* **20,** 851–875.

Mills, G., 1997: An urban canopy-layer climate model. *Theor. Appl. Climatol.,* **57,** 229–244.

Novak, D. R., and B. A. Colle, 2006: Observations of multiple sea breeze boundaries during an unseasonably warm day in metropolitan New York City. *Bull. Amer. Meteor. Soc.,* **87,** 169–174.

Pan, H.-L., and L. Mahrt, 1987: Interaction between soil hydrology and boundary-layer development. *Bound.-Layer Meteor.,* **38,** 185–202.

Pullen, J., T. Holt, A. F. Blumberg, and R. D. Bornstein, 2007: Atmospheric response to local upwelling in the vicinity of New York–New Jersey harbor. *J. Appl. Meteor. Climatol.,* in press.

Rutledge, S. A., and P. V. Hobbs, 1983: The mesoscale and microscale structure and organization of clouds and precipitation in midlatitude cyclones. VIII. A model for the "seeder-feeder" process in warm-frontal rainbands. *J. Atmos. Sci.,* **40,** 1185–1206.

Sailor, D. J., and L. Lu, 2004: A top-down methodology for developing diurnal and seasonal anthropogenic heating profiles for urban areas. *Atmos. Environ.,* **38,** 2737–2748.

Swaid, H., 1993: The role of radiative-convective interaction in creating the microclimate of urban street canyons. *Bound.-Layer Meteor.,* **64,** 231–259.

Tanaka, S., H. Takeda, T. Adechi, and T. Tsuchiya, 1993: *Architectural Environmental Engineering*. Inoue Co., 301 pp.

Thompson, W. T., T. Holt, and J. Pullen, 2007: Investigation of a sea breeze in an urban environment. *Quart. J. Roy. Meteor. Soc.,* in press.

Uno, I., X.-M. Cai, D. G. Steyn, and S. Emori, 1995: A simple extension of the Louis method for rough surface layer modeling. *Bound.-Layer Meteor.,* **76,** 395–409.

Vu, T. C., T. Asaeda, and Y. Ashie, 1999: Development of a numerical model for the evaluation of the urban thermal environment. *J. Wind Eng. Ind. Aerodyn.,* **81,** 181–191.

Yamada, T., 1982: A numerical model study of turbulent airflow in and above a forest canopy. *J. Meteor. Soc. Japan,* **60,** 439–454.